INL/EXT-06-11742

Report to the DOE on the Crud II Project

Dawn E. Janney
Douglas L. Porter
O. Keener Earle
Rick Demmer
Jeffrey J. Giglio
Mark W. Huntley
Michael G. Jones
Joshua L. Peterson

September 2006

The INL is a U.S. Department of Energy National Laboratory
operated by Battelle Energy Alliance

INL/EXT-06-11742

Report to the DOE on the Crud II Project

Dawn E. Janney, Ph.D., Principal Investigator
Douglas L. Porter, Ph.D., Principal Investigator
O. Keener Earle, Project Manager
Rick Demmer
Jeffrey J. Giglio, Ph.D.
Mark W. Huntley
Michael G. Jones
Joshua L. Peterson[a]

[a]Present Address: University of Texas, Austin

September 2006

Center for Nuclear Fuels and Materials Research
Idaho National Laboratory
Idaho Falls, Idaho 83415

Prepared for the
U.S. Department of Energy
Office of Nuclear Energy
Under DOE Idaho Operations Office
Contract DE-AC07-05ID14517

ABSTRACT

Crud (radioactive corrosion products forming in operating reactors) is a major problem for the electric power industry. Conditions leading to its formation are complex and poorly understood, and it is widely recognized that accurate materials characterization of crud is essential to understanding how to prevent it or reduce the operating and health hazards it creates. However, crud samples are difficult to collect and analyze because of their high radioactivity and common formation on activated fuel pins.

This report documents analyses of crud samples from a commercial boiling water reactor that were provided by the Electric Power Research Institute to Idaho National Laboratory (INL) as part of an on-going effort to develop the capabilities of INL to address problems associated with currently operating commercial reactors. The samples represent material collected during two refueling outages. Each sample was analyzed by gamma scanning, atomic absorption spectroscopy, and inductively coupled plasma mass spectroscopy in the Analytical Laboratory at INL. Seven of the samples were also analyzed using optical microscopy in the Electron Microscopy Laboratory at INL. Two of the samples were further analyzed using transmission and scanning electron microscopy and electron diffraction at INL. Although not comprehensive, the electron-microscopy analyses are among the few published examples of similar work in the last several decades.

SUMMARY

Crud (activated corrosion products forming inside reactors) is a major problem in the nuclear power industry. Although it is widely recognized that an accurate characterization of crud is essential, crud samples are difficult to collect and analyze because of their high radioactivity and common formation on activated fuel pins.

This report documents analyses of crud samples from a commercial boiling water reactor that were provided by the Electric Power Research Institute to Idaho National Laboratory (INL) as part of an on-going effort to develop the capabilities of INL to address problems associated with currently operating commercial reactors. The samples represent material collected during two refueling outages. Cycle 16 samples, from a 2-cycle bundle with 22.2 GWD/MTU burnup, were collected by brushing the fuel rods or scraping them with a stone while they were in the pool, then sucking pool water through a mixed cellulose ester filter. Cycle 17 samples, from a one-cycle bundle with 21.9 GWD/MTU burnup, were collected by brushing the rods, scraping them with a knife, and sucking pool water through a wire mesh screen (to catch large particulates) followed by a paper filter.

Each sample was analyzed by gamma scanning, atomic absorption (AA) spectroscopy, and inductively coupled plasma mass spectroscopy (ICP-MS) in the Analytical Laboratory at INL. Seven of the samples were also analyzed using optical microscopy in the Electron Microscopy Laboratory (EML) at INL. Two of the samples were further analyzed using transmission and scanning electron microscopy (TEM and SEM) at INL.

When inspected visually, each of the paper and cellulose filters had a pinkish or purplish color on one side. Particles large enough to be visible using optical microscopy were rare. No particles were observed on the wire mesh screen.

Scanning electron microscopy analysis of a Cycle 16 sample showed numerous small particles with high concentrations of zirconium or of aluminum. A few areas with high concentrations of iron were also found. Detailed SEM analysis of the Cycle 16 sample was not carried out because the cellulose filter deteriorated during observation. Transmission electron microscope (TEM) analyses showed numerous particles of corundum (α-Al_2O_3) and hematite (α-Fe_2O_3). High-zirconium particles were noted, but not analyzed in enough detail to allow identification of a specific crystal structure. Beam-sensitive aluminosilicate particles (probably clays) were also observed in the TEM data.

Scanning electron microscopy analysis of a Cycle 17 sample showed numerous small particles with high concentrations of zirconium, iron, or lead, and larger aluminosilicate particles (one of which had a small high-zirconium particle embedded in it). Transmission electron microscopy showed numerous particles of hematite (α-Fe_2O_3), with wide variations in sizes and shapes. Some of the data suggest the possible presence of small quantities of a spinel-structured iron oxide mineral, possibly including Mn, Zn, or Ni. Small particles with apparent high-Zr and high-Fe layers were observed in both the TEM and SEM data.

ACKNOWLEDGMENTS

The authors would like to thank Dr. Bo Cheng (EPRI) and Dr. Shaw Bian (Energy Northwest), who arranged for the samples described in this report to be provided to the Idaho National Laboratory. Dr. Cheng, Dr. George Sabol (Consultant), and Dr. Mike Pop (Areva) arranged for us to see their unpublished results on other crud samples and provided helpful discussion.

The authors would also like to thank the Center for Nuclear Materials and Fuels Research. Dr. Tom O'Holleran and Mr. Mark Surchik supported work done at the Electron Microscopy Laboratory, and Dr. Marsha Lambregts supported work done at the Analytical Laboratory. Copy editor Heather Rorhbaugh and text processors Penny Simon and Debbie Southwick from the Technical Reports Service provided expert assistance with final document preparation.

Finally, the authors would like to thank Tom Miller, program manager from the sponsoring organization within the DOE Office of Nuclear Energy, which funded this work.

CONTENTS

ABSTRACT iii

SUMMARY v

ACKNOWLEDGMENTS vii

ACRONYMS xv

1. INTRODUCTION 1

2. METHODS 3

3. RESULTS 5

3.1 Cycle 16 5

3.1.1 Optical observations, Cycle 16 5
3.1.2 Scanning electron microscopy, Sample 21 (Cycle 16) 6
3.1.3 Transmission electron microscopy, Sample 21 (Cycle 16) 7
3.1.4 Analytical Laboratory Results, Cycle 16 14

3.2 Cycle 17 15

3.2.1 Optical observations, Cycle 17 15
3.2.2 Scanning electron microscopy, Sample 11 (Cycle 17) 15
3.2.3 Transmission electron microscopy, Sample 11 (Cycle 17) 23
3.2.4 Analytical Laboratory Results, Cycle 17 39

4. DISCUSSION 40

5. REFERENCES 42

Appendix A—Optical Images, Cycle 16 43

Appendix B—Weight percentages from SEM-EDX Spectra, Cycle 16 (Sample 21) 51

Appendix C—Weight percentages from TEM-EDX Spectra, Cycle 16 (Sample 21) 55

Appendix D—Analytical Lab results, Cycle 16 59

Appendix E—Optical Images, Cycle 17 63

Appendix F—Weight Percentages from SEM-EDX Spectra, Cycle 17 (Sample 11) 66

Appendix G—Weight Percentages from TEM-EDX Spectra, Cycle 17 (Sample 11) 72

Appendix H—Analytical Lab Results, Cycle 17 78

FIGURES

1. Optical images, Cycle 16 samples. 5

2. BSE SEM images, Cycle 16 (Sample 21). 6

3. TEM images and diffraction patterns, high-Al material, Cycle 16 (Sample 21) 8

4. TEM image and diffraction patterns of the high-Fe crystal corresponding to spectrum 35, Cycle 16 (Sample 21) 9

5. TEM image of another high-Fe particle, Cycle 16 (Sample 21). 10

6. TEM images and diffraction patterns from three high-Zr particles, Cycle 16 (Sample 21) 12

7. TEM image and diffraction pattern from high-Na material, Cycle 16 (Sample 21) 14

8. Optical images, Cycle 17 samples. 15

9. SEM images showing several areas of small particles, Cycle 17 (Sample 11). 16

10. SEM images of area “C” (9), Cycle 17 (Sample 11) 17

11. SEM images of a raised area in Cycle 17 (Sample 11) and the adjacent filter 18

12. SEM images of a high-Pb area in Cycle 17 (Sample 11) 19

13. EDX Spectra 9 and 10 (Cycle 17, Sample 11) 20

14. SEM images of an aluminosilicate material and adjacent high-Zr material, Cycle 17 (Sample 11) 21

15. SEM images of numerous small particles, Cycle 17 (Sample 11). 22

16. SEM image of a large, high-Zr particle, Cycle 17 (Sample 11) 23

17. TEM data from a cluster of high-Fe particles, Cycle 17 (Sample 11) 24

18. A single iron oxide crystal on the edge of a larger particle, Cycle 17 (Sample 11). 26

19. Three thin areas along the edge of a large particle, Cycle 17 (Sample 11) 27

20. A single electron-transparent crystal along the edge of the large particle shown in Figure19, Cycle 17 (Sample 11) 30

21. A small high-Pb particle, Cycle 17 (Sample 11). 30

22. A small particle with high-Zr and high-Fe areas, Cycle 17 (Sample 11) 32

23. A particle consisting of a large crystal and numerous smaller ones, Cycle 17 (Sample 11) 33

24. A complex particle with numerous dark and light domains, some of which have high concentrations of Na, Al, Cr, or Zn, Cycle 17 (Sample 11). 34

25. A complex particle with numerous domains, some as small as 10 nm across, Cycle 17 (Sample 11). 35

26. A complex particle containing Fe oxides, Fe-Zr phases, and aluminosilicates, Cycle 17 (Sample 11). 36

27. Particle from which Spectrum 39 (Table 27) was collected, Cycle 17 (Sample 11) 38

28. Image of Particle from which Spectrum 40 (Table 28) was collected, Cycle 17 (Sample 11) 39

A1. Optical images, Sample 21 45

A2. Optical images, Sample 21 (continued) 45

A3. Optical images, Sample 22 46

A4. Optical images, Sample 22 (continued) 46

A5. Optical images, Sample 22 (continued) 47

A6. Optical images, Sample 25 47

A7. Optical images, Sample 25 (continued) 48

A8. Optical images, Sample 28 48

A9. Optical images, Sample 28 (continued) 49

A10. Optical images, Sample 29 49

A11. Optical images, Sample 29 (continued) 50

E1. Optical images, Sample 11 65

E2. Optical image, Sample 12 65

TABLES

1. Cycle 16 samples from rods I9 and J6, collected from a 2-cycle bundle (22.2 GWD/MTU burnup) during Refueling Outage R16 1

2. Cycle 17 samples collected from Rod G10 in a one-cycle bundle, 21.9 GWD/MTU burnup, during Refueling Outage R17 2

3. Atomic percentages in high-Zr materials from SEM-EDX spectra, normalized to 100% (Cycle 16, Sample 21) 7

4. Atomic percentages in high-Fe materials from SEM-EDX spectra, normalized to 100% (Cycle 16, Sample 21) 7

5. Atomic percentages in high-aluminum materials from TEM-EDX spectra, normalized to 100% (Cycle 16, Sample 21) 7

6. Atomic percentages in high-iron materials from TEM-EDX spectra, normalized to 100% (Cycle 16, Sample 21) 10

7. Atomic percentages in high-Zr materials from TEM-EDX spectra, normalized to 100% (Cycle 16, Sample 21) 13

8. Atomic percentages in high-Al, high-Si materials from TEM-EDX spectra, normalized to 100% (Cycle 16, Sample 21) 13

9. Atomic percentages in high-Na material from TEM-EDX spectra, normalized to 100% (Cycle 16, Sample 21) 14

10. Atomic percentages from SEM-EDX spectra shown in Figures 9 and 10, normalized to 100% (Cycle 17, Sample 11) 17

11. Atomic percentages from SEM-EDX spectra shown in Figure 11, normalized to 100% (Cycle 17, Sample 11) 18

12. Atomic percentages from spectra shown in Figure 12, normalized to 100% (Cycle 17, Sample 11) 21

13. Atomic percentages from SEM-EDX spectra shown in Figure 14, normalized to 100% (Cycle 17, Sample 11) 21

14. Atomic percentages from SEM-EDX spectra shown in Figure 15, normalized to 100% (Cycle 17, Sample 11) 22

15. Atomic percentages from SEM-EDX Spectrum 28 (Figure 16), normalized to 100% (Cycle 17, Sample 11) 23

16. Atomic percentages from TEM-EDX spectra shown in Figure 17, normalized to 100% (Cycle 17, Sample 11) 25

17. D-spacings (nm) corresponding to reflections in Figure 17c (Cycle 17, Sample 11) 25

18. Atomic percentages from TEM-EDX data from the crystal shown in Figure 18, normalized to 100% (Cycle 17, Sample 11) 26

19. Atomic percentages from TEM-EDX spectra shown in Figures 19 and 20, normalized to 100% (Cycle 17, Sample 11) 28

21. Characteristic x-rays with high relative intensities that have possible peak overlaps with Pb^4 31

22. Atomic percentages from TEM-EDX spectra shown in Figure 22, normalized to 100% (Cycle 17, Sample 11) 32

23. Atomic percentages from TEM-EDX spectra shown in Figure 23, normalized to 100%. (Cycle 17, Sample 11) 33

24 Atomic percentages from TEM-EDX spectra shown in Figure 24, normalized to 100% (Cycle 17, Sample 11) 34

25 Atomic percentages from TEM-EDX spectra shown in Figure 25, normalized to 100% (Cycle 17, Sample 11) 36

26. Atomic percentages from TEM-EDX spectra shown in Figure 26, normalized to 100% (Cycle 17, Sample 11) 37

27. Atomic percentages from the TEM-EDX spectrum shown in Figure 27, normalized to 100% (Cycle 17, Sample 11) 38

28. Atomic percentages from the TEM-EDX spectrum shown in Figure 28, normalized to 100% (Cycle 17, Sample 11) 39

C-1. Weight percentages from TEM-EDX Spectra, Cycle 16 (Sample 21) (Normalized to 100%) 57

D1 Concentrations of analytes from Cycle 16 samples, µg. 61

D2. Activities measured in August 2006 for Cycle 16 samples, µCi 62

F-1. Weight Percentages from SEM-EDXSspectra, Cycle 17 (Sample 11) (Normalized to 100%) 68

G-1. Weight Percentages from TEM-EDX Spectra, Cycle 17 (Sample 11) (Normalized to 100%) 74

H1. Concentrations of analytes from Cycle 17 samples collected on paper filters and blank filter, µg 80

H2. Activities measured in August 2006 for Cycle 17 samples, µCi 80

ACRONYMS

AA	atomic absorption
BSE	back-scattered electron
EDX	energy dispersive x-ray spectroscopy
EML	Electron Microscopy Laboratory
EPRI	Electric Power Research Institute
ICP-MS	inductively coupled plasma mass spectroscopy
ICP-OES	inductively coupled plasma optical-emission spectroscopy
INL	Idaho National Laboratory
SAED	selected-area electron diffraction
SE	secondary electron
SEM	scanning electron microscopy
TEM	transmission electron microscopy

Report to the DOE on the Crud II Project
Center for Nuclear Fuels and Materials Research
Idaho National Laboratory

1. INTRODUCTION

Crud (radioactive corrosion products forming in operating reactors) is a major problem for the electric power industry. Conditions leading to its formation are complex and poorly understood, and it is widely recognized that accurate materials characterization of crud is essential to understanding how to prevent it or reduce the operating and health hazards it creates. However, crud samples are difficult to collect and analyze because of their high radioactivity and common formation on activated fuel pins.

This report details the scanning electron microscopy (SEM), transmission electron microscopy (TEM), and chemical analyses of crud samples from a commercially operated boiling water reactor. The Electric Power Research Institute (EPRI) arranged to have these samples sent to the Idaho National Laboratory (INL) as part of an ongoing project to improve the Department of Energy's ability to address problems in currently operating commercial nuclear reactors.

Eighteen samples were collected during refueling outage R16. Table 1 summarizes characteristics of these samples. Each sample consists of a 0.45 μm mixed cellulose ester filter (Millipore type HA, lot number R1MN18306) containing particulates collected by sucking pool water through the filter. Sample type "P" indicates samples that were collected by brushing the fuel rods, "S" indicates samples that were collected by scraping the sample with a stone, and "V" indicates samples that were collected by sucking pool water through the filter without scraping or brushing. V samples are considered to represent background contamination from the pool water.

Table 1. Cycle 16 samples from rods I9 and J6, collected from a 2-cycle bundle (22.2 GWD/MTU burnup) during Refueling Outage R16.

Sample ID	Sample Type	Rod ID	Span Location, mm
3	V[b]	N/A	N/A
4	B	J6	477
5	B	I9	477
6	B	I9	867
7	B	I9	1430
8	B	I9	1980
9	B	I9	2540
21	S	J6	2540
22	S	I9	2540
23	S	I9	1980
24	S	J6	1980
25	S	J6	1430
26	S	I9	1430
27	S	I9	867
28	S	J6	867
29	S	I9	477
30	S	J6	477
31	V[c]	N/A	N/A

[b] Water sample before crud collection

Another three samples were collected during refueling outage R17. Table 2 summarizes the characteristics of these samples. Crud for analysis was removed from fuel rods by brushing them to remove loose particulates and then scraping with a blade to remove loose flakes. Samples were collected by sucking pool water through a metal screen to catch any large flakes, then through a hardened ashless paper filter with nominal 8 μm retention (Millipore grade 233, 47 mm diameter). In Table 2, "Screen" samples are metal screens and "Filter" samples are paper filters.

Samples 11, 12, 21, 22, 25, 28, and 29 were selected for optical analysis in the Electron Microscopy Laboratory (EML). Small portions of Samples 11 and 21 were further analyzed using transmission and scanning electron microscopy (TEM and SEM) in the EML. All of the samples listed in Tables 1 and 2 were sent to the Analytical Laboratory for chemical analyses.

Table 2. Cycle 17 samples collected from Rod G10 in a one-cycle bundle, 21.9 GWD/MTU burnup, during Refueling Outage R17.

Sample ID	Sample Type	Span Location
10	Filter	Midspan 3
11	Filter	Midspan 7
12	Screen	Midspan 7

[c] Water sample after crud collection

2. METHODS

Two or three pieces of filter from each of the samples selected for electron microscopy were prepared by cutting out small pieces of screen or paper filter with scissors or breaking and tearing off small pieces of cellulose filters with tweezers. Each piece was approximately ¼ to ½ cm across. Samples for optical and SEM analysis were mounted on high-purity carbon sticky dots (Ted Pella part number 16084-4)[d] on aluminum SEM stubs.

Optical analysis was carried out by examining each piece of material that had been mounted on an SEM stub with a Leica MZ12 microscope equipped with a Paxcam digital camera (model PX-CM) and Pax-It software (Version 6).

After optical analysis, one SEM stub from Sample 11 and one from Sample 21 were mounted in an aluminum-foil-coated block. Pieces of copper tape were placed on the foil next to the stubs for X-ray spectroscopy calibration. The entire block was coated with Pd to reduce electrostatic charge buildup during analysis.

Scanning electron microscope energy-dispersive x-ray spectroscopy (SEM-EDX) data and electron images from material on SEM stubs were collected using a Zeiss DSM960A scanning electron microscope equipped with an Oxford Link Isis EDX detector and Link Isis software. The microscope was operated at 20 kV. Despite the Pd coating, artifacts from electrostatic charging are visible in some back-scattered electron (BSE) images, and this charging generally prevented successful collection of secondary electron (SE) images.

Caution must be used in interpreting the SEM-EDX spectra as representing single particles for two reasons:

1. The EDX spectra were collected using a working distance of 25 mm, while the images were collected with a working distance of 10-15 mm to obtain sharp focus at the magnifications required to observe individual particles. Thus, the beam used to collect the spectrum may not have been centered in the precise area indicated.

2. The spatial resolution of SEM-EDX data is governed by the volume of the sample interacting with the beam, including absorption of, and fluorescence by, characteristic x-rays that do not immediately leave the sample. Although the precise size and shape of the interaction volume are poorly known in geometrically complex samples such as those examined here, the spatial resolution of an EDX analysis is likely to be on the order of several micrometers.

TEM samples were prepared by placing small amounts of filter material with attached crud in 10-15 ml of pure water, ultrasonicating for several hours, placing a drop of the water on a commercially available carbon-coated formvar film supported by a 300-mesh Au TEM grid, and air drying. All TEM data were collected using a JEOL 2010 microscope operating at 200 kV. Images and selected-area electron-diffraction (SAED) patterns were collected using a Gatan Ultrascan camera and Digital Micrograph software (v. 3.10 for GMS 1.5.0). Reflection spacings in diffraction patterns were converted

---

[d] PRODUCT DISCLAIMER

References herein to any specific commercial product, process, or service by trade name, trademark, manufacturer, or otherwise, does not necessarily constitute or imply its endorsement, recommendation, or favoring by the U.S. Government, any agency thereof, or any company affiliated with the Idaho National Laboratory.

to d-spacings using an empirically determined camera constant obtained from diffraction patterns of nanocrystalline gold taken using lens settings similar to those used to collect the data in this report. Phases producing diffraction patterns with rings were identified by comparison to d-spacings and relative intensities in the PDF4+ database (International Centre for Diffraction Data). Other phase-identification criteria are the same as previously used for other crud samples at INL.[1]

Transmission electron microscope energy-dispersive x-ray (TEM-EDX) spectra were collected using an Oxford Link Petafet EDX detector with a SiLi crystal, nominal 20 eV channel width, nominal energy range from 0 to 20 keV, and nominal 136 eV resolution. The spectra were collected and quantified using Link Isis software, Isis Suite revision 3.2, with peak profiles and k-factors supplied by the manufacturer. Unless otherwise specified, each spectrum was collected with a nominal beam diameter of 15 to 25 nm. Each spectrum was quantified individually based on a qualitative analysis including peaks identified from visual inspection of the spectrum.

For sufficiently thin samples, there is little absorption, fluorescence, or beam broadening,[2] thus, spatial resolution in TEM-EDX analyses for these samples is commonly assumed to be approximately the beam diameter. However, the universal presence of peaks from the Au grid in the EDX spectra in this study indicates that each spectrum includes x-rays from materials outside the beam. Some of these x-rays may be produced by electrons that have been scattered by the specimen, and others may be generated when x-rays generated by specimen-beam interactions cause surrounding materials to fluoresce.[3] These problems are particularly apparent in spectra collected from, or close to, materials that are too thick to be electron transparent. Extensive experience with the microscope and specimen holder used to collect the data presented here indicates that small peaks from the Fe Kα and Co Kα peaks appear in spectra in which these elements are not present. Similar small peaks were ignored in this study.

Quantification of both TEM- and SEM-EDX spectra is complicated by peak overlaps between the Na K and Zn Lα peaks (at 1.041 and 1.012 keV, respectively), the F K and Fe Lα peaks (at 0.6768 and 0.7050 keV), and the P K and Zr Lα peaks (2.014 and 2.042 keV).[4] Thus, concentrations of Na in spectra that also contained significant concentrations of Zn, of F in spectra with Fe, and of P in spectra with Zr are likely to be inaccurate. Similarly, small peaks from Na, F, and P K-series x-rays could easily be overlooked qualitatively in spectra with large overlapping peaks from L-series x-rays. The appendixes list x-rays used for quantification of each element in each spectrum. Quantification of oxygen was not attempted because it is readily absorbed even in thin samples and the detailed information about sample thickness and density that would be required to correct for absorption is not available.

All of the samples were sent to the Analytical Laboratory at INL for elemental and gamma scan analyses. Each sample was dissolved in boiling nitric acid, to which a small amount of hydrofluoric acid had been added. The resulting liquid was cloudy, indicating the dissolution was incomplete. Also, the wire mesh filter did not dissolve completely.

Because the inductively coupled plasma optical-emission spectroscopy (ICP-OES) instrument was out of commission when the analyses were performed, elemental concentrations were measured using a combination of atomic absorption (AA) spectroscopy for K, Na, and Ca and inductively coupled plasma mass spectroscopy (ICP-MS). Neither of these instruments was capable of measuring iron in the concentrations present in these samples.

3. RESULTS

3.1 Cycle 16

3.1.1 Optical observations, Cycle 16

Cycle 16 filters appear pale pinkish purple on one side and white on the other. Material from the interiors of the filters visible at broken or torn areas at the edges of the sampled pieces are white, suggesting that the crud may be concentrated almost entirely on one surface of the filters. Optical microscope images of broken areas confirm that these surfaces contain few visible particles.

Optical microscope images of the pink side of Cycle 16 samples (Figure 1 and Appendix A) show numerous particles, none of which are large enough to be readily visible as individuals at the available magnifications. The filters have hard surfaces, with numerous dents and scratches (probably from tweezers used during sample preparation). Some filters have relatively uniform particle distributions (e.g., Figure 1a), while others have large, sharp, approximately linear discontinuities (e.g., Figure 1b and c). Many particles have small rounded areas that appear unusually red (e.g., Figure 1d) and may represent localized deposits of a single phase.

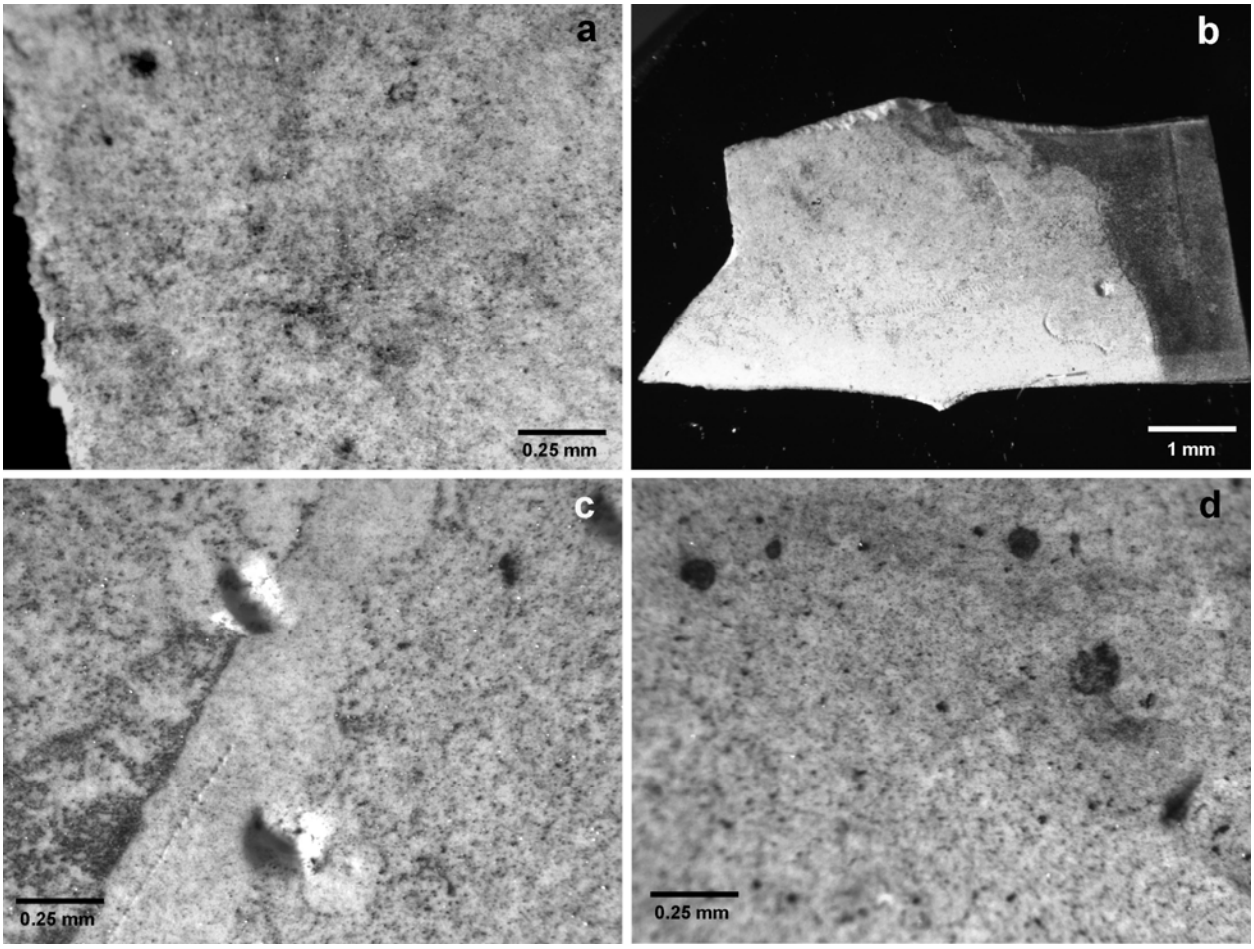

Figure 1. Optical images, Cycle 16 samples. a) Sample 21, showing relatively homogeneous distribution of small particles; b and c) Sample 22, showing linear discontinuities in particle distribution; d) Sample 25, showing numerous rounded dark areas. See Appendix A for other examples.

The optical images suggest that the large discontinuities represent differences in numbers of particles in a given area rather than differences in particle sizes. Because of the way the samples were collected, the discontinuities are assumed to have formed during drying and thus probably do not represent differences in phase assemblages. However, these discontinuities did not appear in the SEM samples from Sample 21, and thus were not examined in detail.

3.1.2 Scanning electron microscopy, Sample 21 (Cycle 16)

SEM was used to survey particle sizes and compositions in Sample 21. As the images in Figure 2 show, the sample contains numerous particles that are at most a few micrometers across. Comparison of back-scattered electron (BSE) images and EDX data collected with a stationary small beam shows that dark-colored particles (Spectra 30, 33, 35, and 39, Figure 2) are qualitatively pure Al (possibly with light elements). Light-colored particles (Spectra 29, 31, 32, and 36-38, Figure 2 and Table 3) have high concentrations of Zr. Particles and areas with intermediate brightness are far less common, but correspond to high-Fe compositions (Spectra 34 and 40, Figure 2 and Table 4). Spectra containing more than one element may represent analyses from several particles.

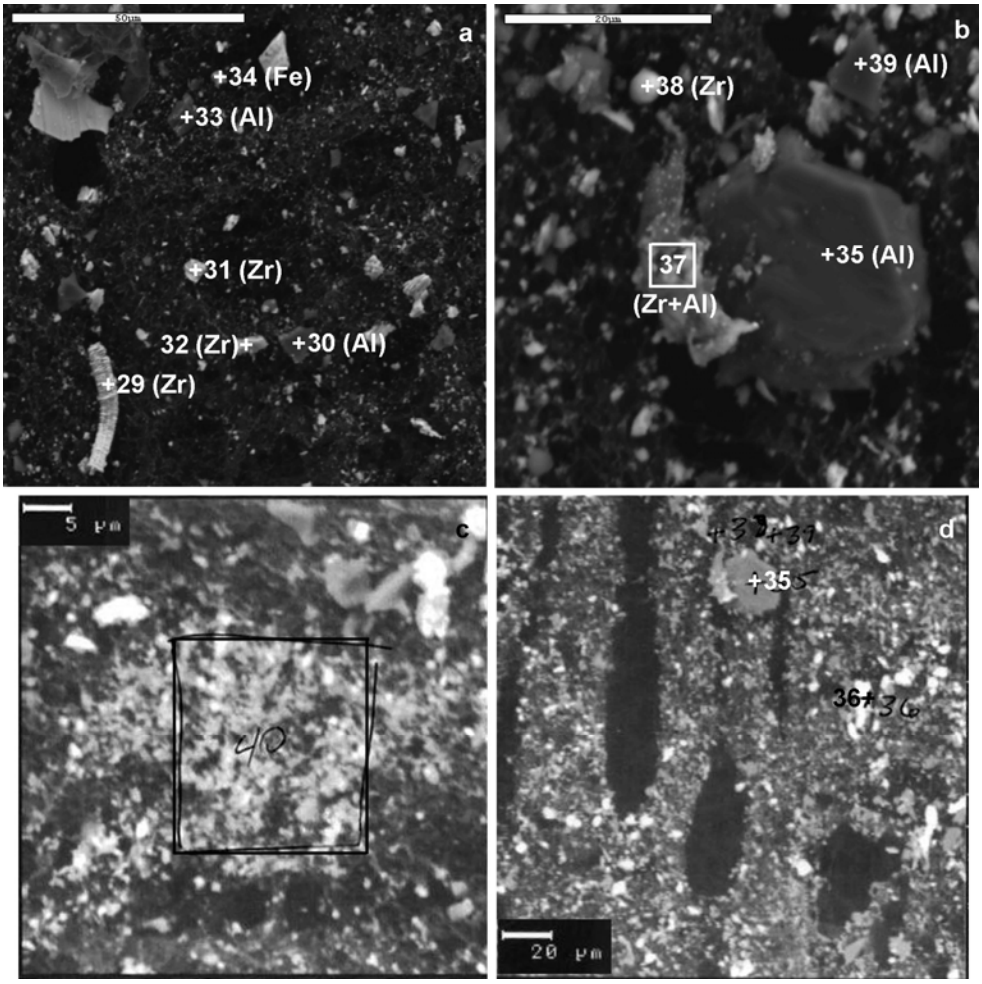

Figure 2. SEM BSE images, Cycle 16 (Sample 21). Numbers correspond to locations of EDX spectra in Tables 3 and 4. a and b) Images showing typical particles. c) Image of a large area of intermediate contrast. Spectrum 40 was collected by rastering the beam over the area included in the box. d) Elongated holes formed during SEM examination.

Table 3. Atomic percentages in high-Zr materials from SEM-EDX spectra, normalized to 100% (Cycle 16, Sample 21).

	Spectrum					
Element	29	31	32	36	37	38
Al		1.1	2.5	5.8	27.5	4.3
Si				0.7	3.2	
Zr	100.0	98.9	97.5	93.5	69.3	95.7

Table 4. Atomic percentages in high-Fe materials from SEM-EDX spectra, normalized to 100% (Cycle 16, Sample 21).

	Spectrum	
Element	34	40
Al	3.3	17.4
Si	1.8	5.2
Fe	92.9	55.6
Ni		2.6
Zr	2.0	19.2

The filter material is somewhat beam-sensitive, and particles commonly appear to drift slowly across the field of view when observed at high magnification. Low-magnification images show elongated holes that developed during observation (Figure 2d).

Because of the small particle size, large proportion of aluminum and zirconium particles (neither very useful for understanding crud) and concerns that volatile materials released during the degradation of the filter might damage SEM detectors, no further SEM data were collected from Cycle 16 samples.

3.1.3 Transmission electron microscopy, Sample 21 (Cycle 16)

TEM was used to identify phases in eight individual particles and an ill-defined material from Sample 21. Two of the particles are corundum (α-Al_2O_3), two are predominantly hematite (α-Fe_2O_3), three are high-Zr materials (probably cladding fragments, possibly with small amounts of attached crud), and one has high concentrations of both Al and Si. Data were also collected from a material consisting of Na with a significant concentration of Si.

3.1.3.1 Corundum. Table 5 shows EDX data from two particles. Each contains predominantly Al; however, low concentrations of Na, Si, Cl, Sr, and Zr were observed in at least one of the spectra. Although oxygen was not quantified, it is qualitatively present in all of the spectra.

Images of the high-Al material (Figure 3a, b) show a highly crystalline material with locally variable deformation. Diffraction patterns show either multiple closely spaced reflections at the same distance from the center of the diffraction pattern (Figure 3c) or short arcs (Figure 3d, e), consistent with the deformation suggested by the images. All three of the diffraction patterns from this material are consistent with an identification of corundum, α-Al_2O_3.

This material probably corresponds to the high-Al spectra in the SEM data from this sample. It may represent small fragments of the “stone” knife used to scrape the fuel pins during sample collection.

Table 5. Atomic percentages in high-aluminum materials from TEM-EDX spectra, normalized to 100% (Cycle 16, Sample 21).

	Spectrum		
Element	9	36	37
Na	6.4		
Al	87.2	97.4	98.4
Si	3.5	2.4	1.6
Cl	0.6		
Sr	0.1		
Zr	2.2	0.2	

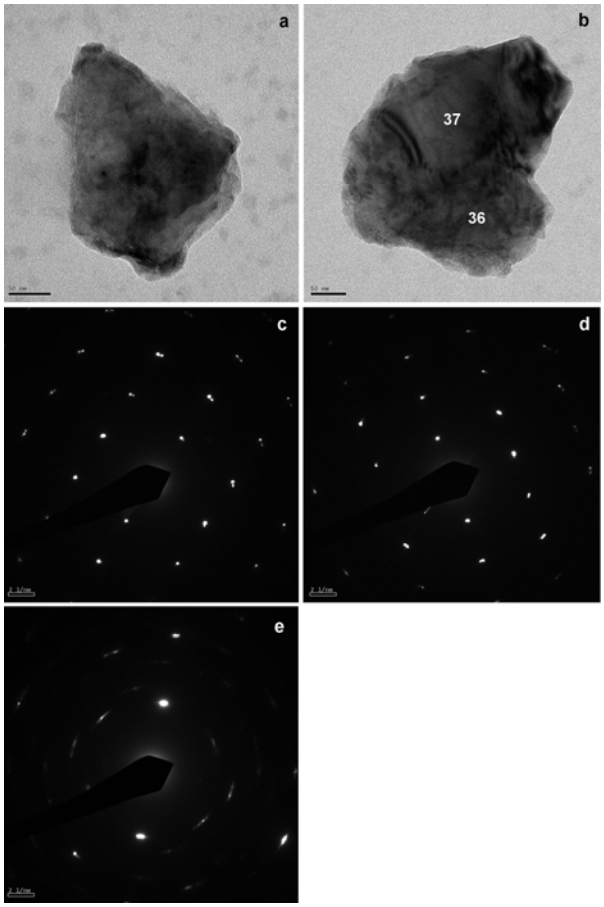

Figure 3. TEM images and diffraction patterns, high-Al material, Cycle 16 (Sample 21). EDX spectra are in Table 5. a) Image of particle from which Spectrum 9 was collected, scale bar: 50 nm. b) Image of particle showing locations from which Spectra 36 and 37 were collected, scale bar: 50 nm. c) and d) Diffraction patterns from particle shown in part a. e) Diffraction pattern from particle shown in part b. Note multiple or tangentially smeared reflections in all diffraction patterns.

3.1.3.2 High-iron materials. Figure 4 shows an image and three diffraction patterns from a single crystal. The corresponding EDX spectrum (Spectrum 35, Table 6) shows a significant concentration of oxygen and suggests that this particle is a nearly pure iron oxide or hydroxide. Each of the diffraction patterns (Figure 4b-d) is consistent with an identification of hematite (α-Fe_2O_3) (assuming that symmetrically forbidden reflections may appear, as they do in single-crystal diffraction patterns from hematite in other crud samples[1]), and at least one of the diffraction patterns could not be produced by magnetite (Fe_3O_4), lepidocrocite (γ-FeOOH), or goethite (α-FeOOH).

Spectra 38-41 (Table 6) and Figure 5 show data from a second high-iron particle. All EDX spectra have large oxygen peaks. In addition to Fe, the spectra show significant concentrations of Na, Al, and Si (in all but one spectrum), as well as much lower concentrations of Cl and several other cations. Proportions of these cations vary widely between the different spectra, suggesting that the cations may be present in different phases.

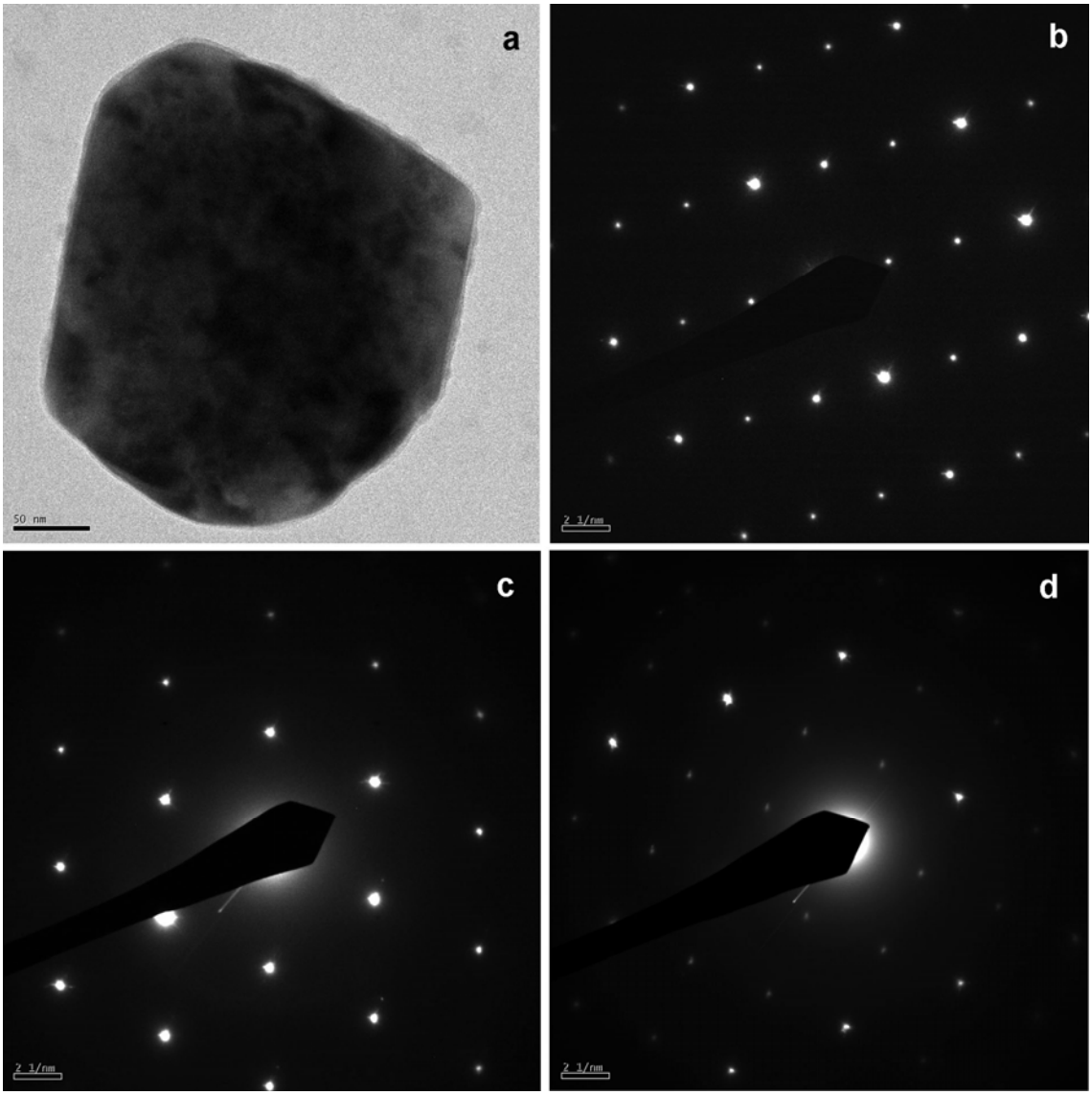

Figure 4.TEM image and diffraction patterns of the high-Fe crystal corresponding to spectrum 35, Cycle 16 (Sample 21) (Table 6).a) Image, scale bar: 50 nm. b-d) Single-crystal diffraction patterns.

Table 6. Atomic percentages in high-iron materials from TEM-EDX spectra, normalized to 100% (Cycle 16, Sample 21).

	Spectrum				
Element	35	38	39	40	41
Na		14.5	15.3	11.1	8.9
Al	0.1	5.7	3.4	6.0	6.3
Si	1.4	6.8	25.2		20.0
Cl		1.7	4.7	2.0	
K		0.7	1.6	0.6	2.4
Ca		1.7	3.3	3.3	3.1
Fe	97.5	52.3	46.4	69.6	59.0
Ni	0.5	2.1			
Cu	0.2	1.8		2.2	
Zn		1.1			
Sr		0.3	0.2	0.7	0.3
Zr	0.3	9.7		1.6	
Ba		1.6		3.0	

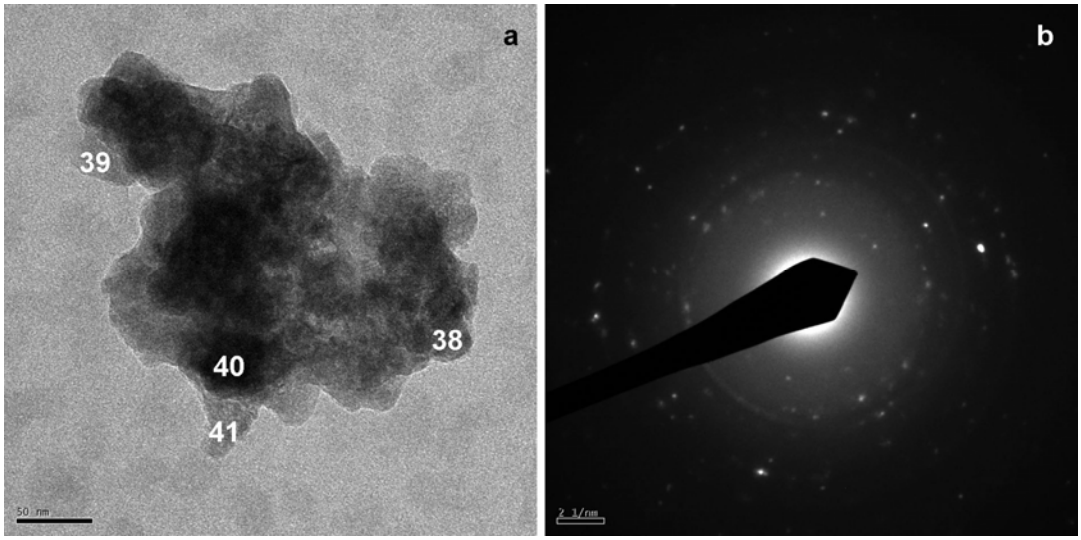

Figure 5. TEM image of another high-Fe particle showing locations of EDX spectra 38-41 (Table 6) and the corresponding diffraction pattern, Cycle 16 (Sample 21). a) Image, scale bar: 50 nm. b) Corresponding diffraction pattern.

The diffraction pattern (Figure 5b) shows numerous individual reflections corresponding to d-spacings of approximately 0.149, 0.160, 0.221, 0.252, 0.268, and 0.365 nm, in apparently random arrangements. In combination with the EDX data, these characteristics suggest that the particle is polycrystalline and may contain at least four phases: one or more iron oxides, an aluminum-bearing

phase, a silicate, and a sodium-bearing phase. Large concentrations of iron in all of the spectra suggest that the iron oxide is the most common phase, which is likely to be well represented in the diffraction pattern. Hematite (α-Fe_2O_3) is the only iron oxide likely to produce high-intensity reflections corresponding to all of the measured d-spacings, and is thus probably present in this particle.

The presence of Zr in two of the high-Fe spectra may indicate that the particle also contains small amounts of cladding, either because the entire particle represents material formed on the outer surface of the cladding or the particle represents an agglomeration of smaller particles that became attached to one another as the sample dried.

3.1.3.3 High-Zr materials. Figure 6 shows images and diffraction patterns from three small particles in which the EDX spectra (Table 7) indicate that Zr is present in the highest concentration of any element quantified. Oxygen is qualitatively present in all of the EDX spectra.

Two of the three diffraction patterns (Figure 6 b, d) have broad, diffuse rings and numerous reflections in an apparently random pattern, suggesting a polycrystalline or amorphous material. The images are consistent with the occurrence of areas with numerous crystallographic domains.

The third diffraction pattern (Figure 6f) does not have diffuse rings. Although numerous reflections are present, many of the reflections are at approximately the same distances from the center of the diffraction pattern. Angular relationships between these reflections suggest that most of the diffraction pattern may represent a single, highly deformed crystal. Moiré fringes (examples at arrows in Figure 6e), which occur when two crystal lattices are superimposed on one another, are common in the image and consistent with the interpretation of the diffraction pattern.

In addition to Zr, many of the EDX spectra in Table 7 show significant concentrations of Na, Al, Si, or Fe. Although data from the ASM Alloy Center suggest that Zircaloy contains a fraction of a weight percent Fe, it apparently does not contain Na, Al, or Si. Further, concentrations of Fe from these EDX spectra appear higher than would be expected if the particles were simply oxidized Zircaloy, and it is likely that the Zr and other elements are in separate phases. Unfortunately, little information about the structure of the particle can be obtained from the image in Figure 6e.

3.1.3.4 High-Al, high-Si material. Two EDX spectra (Table 8) were collected from a high-Al, high-Si particle that became amorphous during TEM observation. Oxygen is qualitatively present in both spectra. Although the material could not be conclusively identified without diffraction data, it is probably a clay.

3.1.3.5 High-Na material. One area with high-Na, high-Si material was also observed in the sample (Figure 7). (Boundaries of this area are sufficiently indistinct that it may not be appropriate to call it a “particle.”) Table 9 shows the composition of this material, the only one observed in this study to have a significant concentration of Cl. Oxygen is qualitatively present in this spectrum. The diffraction pattern (Figure 7b) shows two bright reflections and several fainter, very diffuse ones, but does not provide enough information to identify the phase(s) it represents.

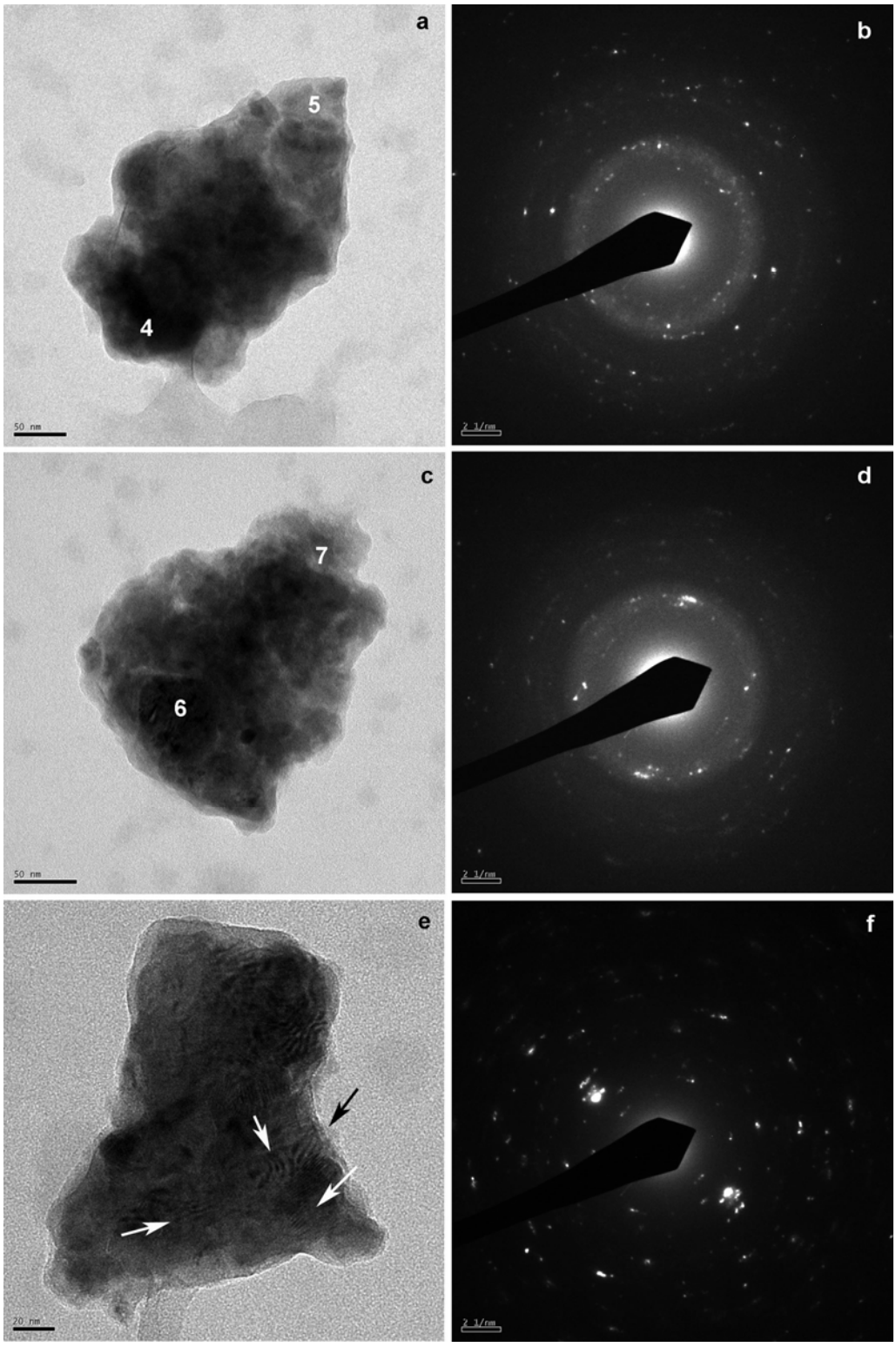

Figure 6. TEM images and diffraction patterns from three high-Zr particles, Cycle 16 (Sample 21). Numbers show locations of EDX spectra in Table 7. a) Image, scale bar: 50 nm. b) Diffraction pattern corresponding to a. c) Image, scale bar: 50 nm. d) Diffraction pattern corresponding to b. e) Image, scale bar: 20 nm. f) Diffraction pattern corresponding to e.

Table 7. Atomic percentages in high-Zr materials from TEM-EDX spectra, normalized to 100% (Cycle 16, Sample 21).

	Spectrum				
Element	4	5	6	7	34
Na	9.3	18.2	5.9	15.0	
Al	3.6	5.7	1.6	5.6	
Si	7.2	23.0	5.4	17.9	
Ca	1.7	3.6			
Fe	9.6	10.7	7.4	14.9	13.1
Ni	0.9				
Cu	0.6				1.7
Zn	0.4				
Sr		0.5		0.4	
Zr	66.7	38.3	79.8	46.2	85.2

Table 8. Atomic percentages in high-Al, high-Si materials from TEM-EDX spectra, normalized to 100% (Cycle 16, Sample 21).

	Spectrum	
Element	2	3
Na		6.2
Al	19.0	24.4
Si	76.4	61.0
Ca	4.6	7.8
Sr		0.6

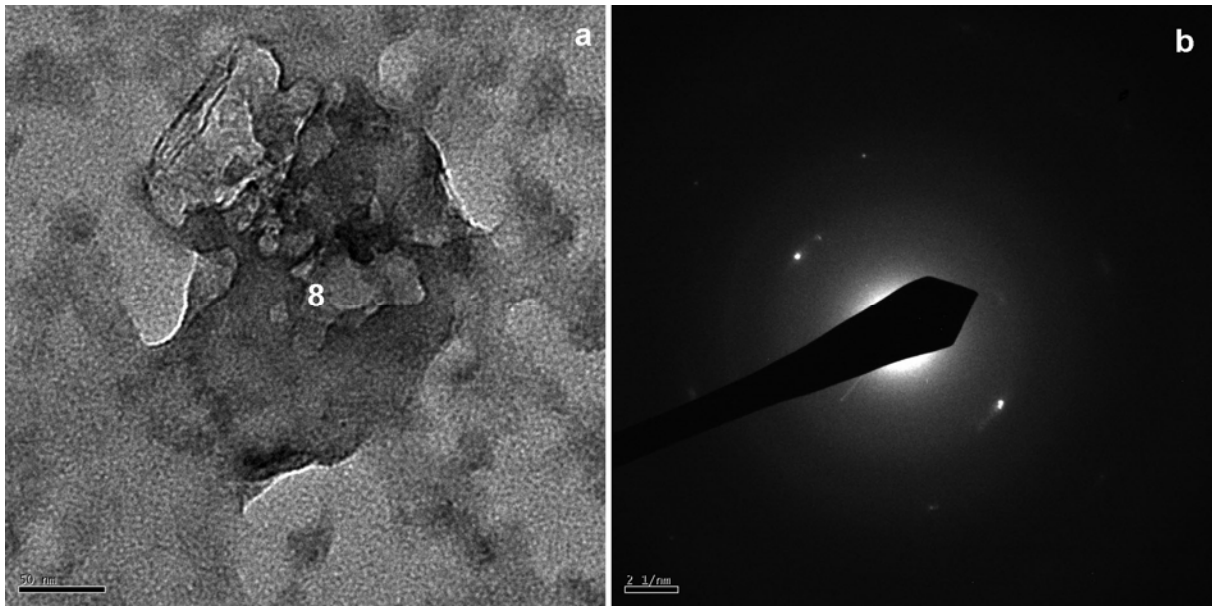

Figure 7. TEM image and diffraction pattern from high-Na material, Cycle 16 (Sample 21) (Table 9). a) Image, scale bar: 50 nm. b) Corresponding diffraction pattern.

Table 9. Atomic percentages in high-Na material from TEM-EDX spectra, normalized to 100% (Cycle 16, Sample 21).

Element	Spectrum 8
Na	51.0
Al	1.5
Si	29.2
Cl	14.5
Ca	3.1
Sr	0.8

3.1.4 Analytical Laboratory Results, Cycle 16

Elemental concentrations from Cycle 16 samples are reported in Appendix D. Concentrations of Cr, Mn, and Ni are consistently higher in Samples 4-30, which are associated with crud from specific fuel pins and locations, than in Samples 3 and 31, which represent pool water, suggesting that these elements are from the crud. Concentrations of Mo and Zn present a less consistent pattern, in which concentrations in crud samples are either below detection limits for these elements (0.4 and 20 μg, respectively) or well above those of pool samples.

Concentrations of Cr, Mn, Ni, Mo, Ni, and Zn are generally higher in Samples 21-30, which were collected by scraping the fuel rods with a stone knife, than in Samples 4-9, which were collected by brushing the fuel rods. Assuming that total quantities of crud are similar in all samples, this comparison suggests that scraping may be a more effective way to collect crud than brushing.

The SEM and TEM data suggest that Zr is present as a discrete phase (probably representing the outer surface of the cladding). Thus, variations in Zr concentrations probably reflect differences in the proportions of crud and cladding in the samples rather than differences in crud composition. This interpretation is consistent with the generally much higher concentrations of Zr in Samples 21-30, which were collected by scraping the fuel rods with a stone knife, than in Samples 4-9, which were collected by brushing the fuel rods.

Values of Al are lower than would have been expected from the Sample 21 SEM and TEM data. Corundum (α-Al_2O_3) is highly resistant to dissolution. It probably would not have dissolved during sample preparation. Thus, it is likely that much of the corundum remained as fine particulates and was filtered out before chemical analysis. Reported aluminum concentrations may thus reflect primarily dissolution of any aluminosilicates.

3.2 Cycle 17

3.2.1 Optical observations, Cycle 17

One side of Sample 11 (a paper filter) was very pale pink, with a white rim around the outer edge. Optical images of this sample (Figure 8, Appendix E) show a fibrous texture with small, sparsely distributed dark areas. No individual particles could be distinguished.

No particles were observed on Sample 12, a wire screen (Figure 8, Appendix E).

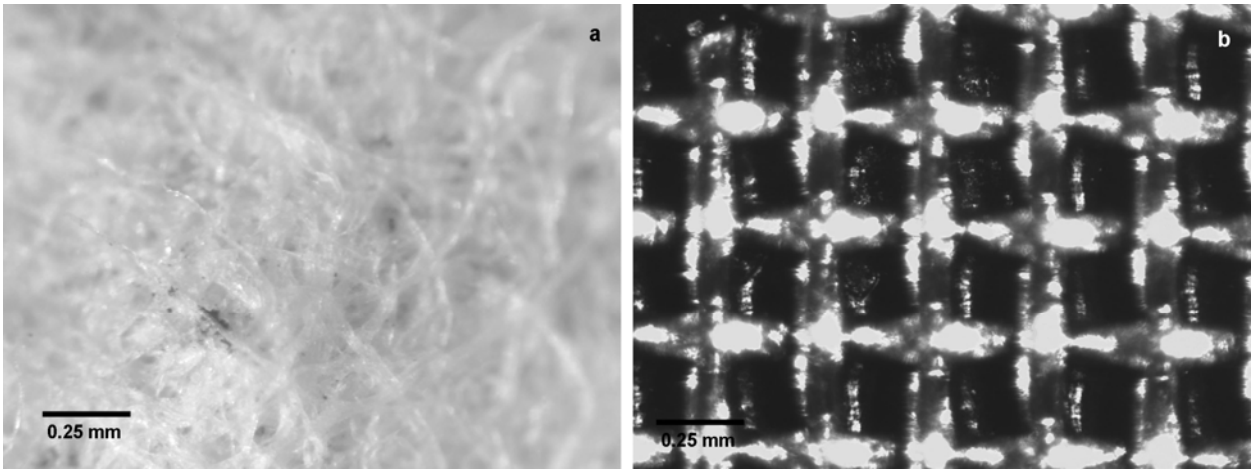

Figure 8. Optical images, Cycle 17 samples. a) Sample 11, showing fibrous nature of the filter and small dark areas along a fiber. b) Sample 12, showing wire screen without particles. See Appendix E for other examples.

3.2.2 Scanning electron microscopy, Sample 11 (Cycle 17)

Scanning electron microscope images and EDX spectra were collected from several areas of Sample 11. Because optical observations showed no particles on Sample 12, SEM analysis of this sample was not carried out.

Figures 9 and 10 show the typical fibrous texture of the substrate in Sample 11, with the letters "A," "B," and "C" indicating examples of small particles apparently attached to individual fibers. Many particles are less than 1 μm across.

Table 10 gives compositions from EDX spectra whose approximate locations are shown in Figures 9 and 10. Spectrum 1 apparently represents a pure Fe oxide or hydroxide, while 3 consists primarily of Zr. Figure 9d suggests that Spectrum 4 is from a collection of sub-micron particles, and therefore may represent a mixture of high-Fe and high-Zr phases.

Figure 10 emphasizes a large (tens of μm), lumpy particle consisting primarily of a material with contrast similar to that of the filter in BSE images, but with small high-contrast areas. Spectrum 2 is from the low-contrast material, which is an aluminosilicate with an Al:Si ratio slightly greater than 1:2. Figure 10c and Spectrum 5, emphasizing one of the high-contrast areas and its relationship to its surroundings, show that the high-contrast area is a small particle of high-Zr material. The EDX data, lumpy appearance, and incorporation of high-Zr areas suggest that the particle shown in Figure 10 consists of an aggregate of clay that incorporated small particles of Zr as it formed.

Figure 11 shows a part of the specimen that appears slightly raised above the surface of a fiber in the filter. In this area, a thin layer of a material that appears bright in BSE images may be superimposed on a layer of a material with contrast similar to that of the filter. Compositions corresponding to EDX Spectra 6 and 7, which are from the raised area, are in Table 11. Spectrum 8, from the area shown by the box in Figure 11, represents the composition of the filter paper and confirms that the filter is not the source of the Fe and Ni shown in Table 11.

Figure 9. SEM images showing several areas of small particles, Cycle 17 (Sample 11). a) Overview; particles from areas labeled “A,” “B,” and “C” were studied in detail. BSE image, scale bar: 50 μm. b) Higher magnification view of area “A.” BSE image, scale bar: 20 μm. c) Higher magnification view of small particles in area “A,” showing approximate location of spectrum 1 (Table 10). SE image, scale bar: 2 μm. d) Area “B,” showing approximate locations of spectra 3 and 4 (Table 10). BSE image, scale bar: 5 μm.

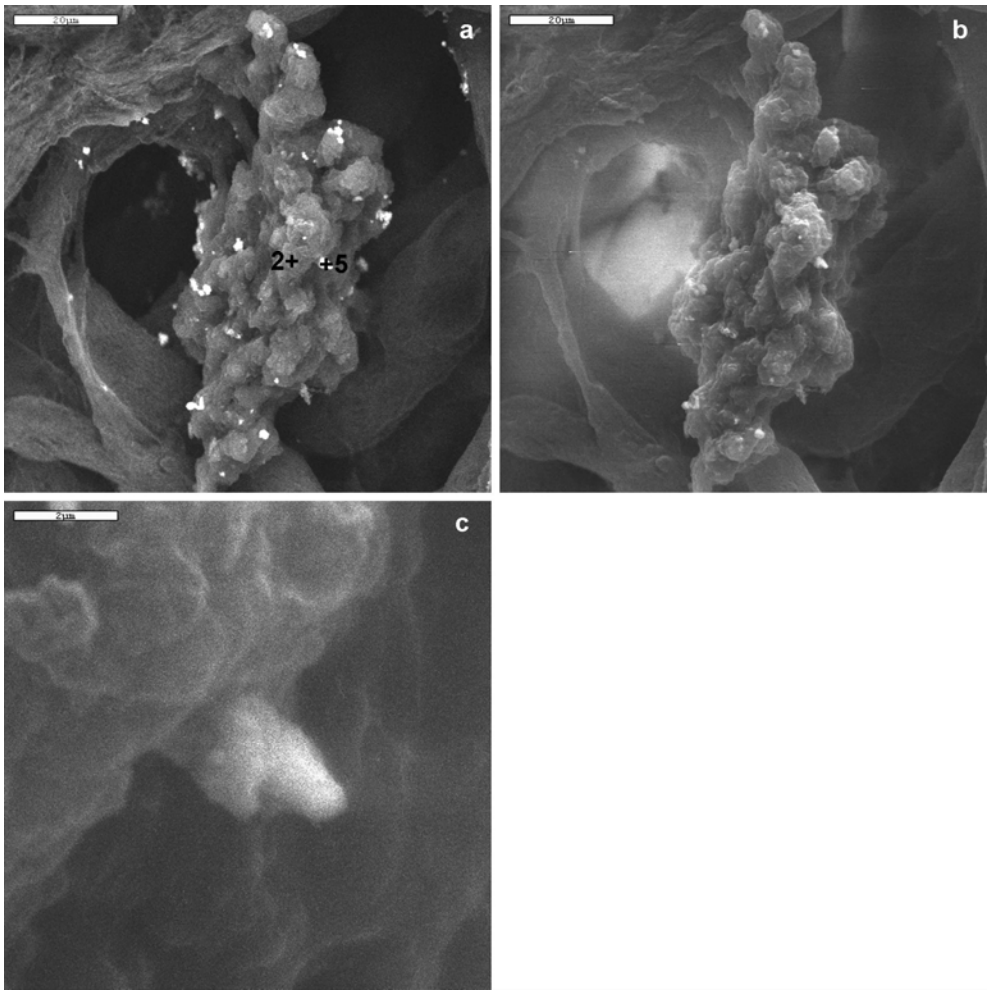

Figure 10. SEM images of area "C" (Figure 9), Cycle 17 (Sample 11). a) Overview of particle, showing approximate locations of spectra 2 and 5 (Table 10). BSE image, scale bar: 20 µm. b) SE image corresponding to part a, emphasizing "lumpy" surface of particle. Scale bar: 20 µm. c) Higher-magnification image showing a small area that appears bright in BSE images and its relationship to the remainder of the particle. Spectrum 5 was collected from the bright area. BSE image, scale bar: 2 µm.

Table 10. Atomic percentages from SEM-EDX spectra shown in Figures 9 and 10, normalized to 100% (Cycle 17, Sample 11).

	Spectrum				
Element	1	2	3	4	5
Al		37.0			3.2
Si		63.0			
Fe	100		3.9	29.6	21.9
Zn				2.7	
Zr			91.6	67. 7	74.9
Sn			4.5		

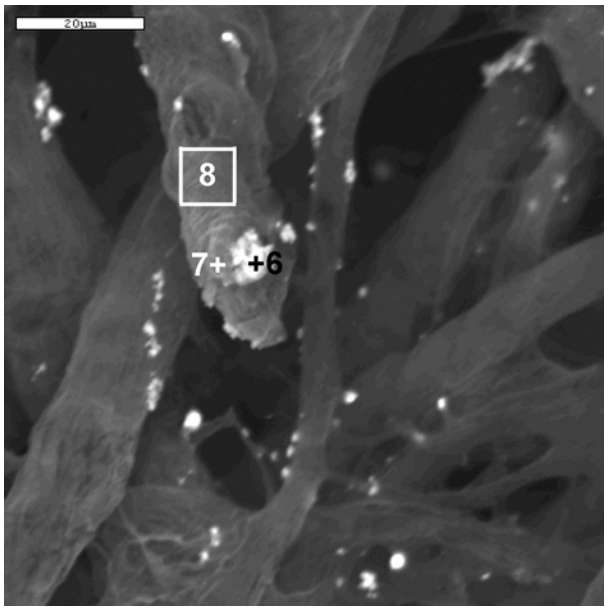

Figure 11. SEM images of a raised area in Cycle 17 (Sample 11) and the adjacent filter. Numbers indicate approximate locations of Spectra 6 and 7 (Table 11); Spectrum 8 (from the filter itself) was collected for comparison and shows only C and Pd peaks. BSE image, scale bar: 20 µm.

Table 11. Atomic percentages from SEM-EDX spectra shown in Figure 11, normalized to 100% (Cycle 17, Sample 11).

	Spectrum	
Element	6	7
Fe	82.7	100
Ni	17.3	

If taken at face value, the data in Table 11 suggest that the raised area in Figure 11 consists of an area of an iron-nickel alloy (possibly with light elements) adjacent to or on top of an area of essentially pure iron (possibly with light elements in both cases). However, the similarity in contrast between the carbon filter (Spectrum 8, which shows only peaks from C and Pd) and the high-iron material in Spectrum 7 is puzzling. It suggests a greater similarity in atomic numbers between the areas sampled by Spectra 7 and 8 and a greater difference between Spectra 6 and 7 than are indicated by the EDX data.

Figure 12 shows a small bright area whose EDX spectra (Figure 13, Table 12) indicate that it consists of Pb and Si. Quantification of Pb is based on Pb M-series characteristic x-rays, and is complicated by an overlap between the Pb Mα, S Kα, and Mo Lα x-rays (at 2.3455, 2.307 and 2.290 KeV, respectively).[4] The Pb was qualitatively identified by the presence of the Pb Lα x-ray (10.55 KeV; Spectrum 10 also has a peak from the Pb Lβ x-ray, which was used to resolve a possible overlap between the Pb Lα and As Kα x-rays). However, it remains possible that the areas represented by the EDX spectra in Table 12 also include S or Mo.

Figure 14 shows adjacent areas of an aluminosilicate material (EDX Spectra 11 and 12, Table 13) and several thin pieces of a high-Zr material with a striated surface (Spectra 16-18). The composition and appearance of the aluminosilicate material suggest that it is clay similar to that in Spectrum 5. The high-Zr material is probably part of the cladding; the reason for the thin, flaky morphology and conspicuous

striations is unclear. Figure 14b, which shows the interface between the aluminosilicate and high-Zr material, suggests that these materials touch one another, but are not intergrown.

Figure 15 shows another area, in which several small particles form a row along the edge of a curved fiber. Contrast variations between the right and left edges of the particles in high-magnification images suggest compositional layers within each particle. The thickness of each layer is approximately the spatial resolution of each EDX analysis, and small errors in positioning the beam are likely because of the poor image quality at the working distance required to collect the EDX data, so it is likely that each analysis represents both materials in different proportions. Nonetheless, EDX Spectra 21 and 22 (from areas that look dark in BSE images) have higher concentrations of Fe, and lower concentrations of Ni, Zn, and Zr, than Spectra 20, 23, and 24 (all from areas that look bright). These observations suggest that the particles in the row are minuscule "flakes," in the sense that each contains the extreme outer part of the cladding and the immediately adjacent part of the crud.

Spectra 25-27 are from nearby small particles and show varying proportions of Fe, Ni, Zn, and Zr. However, none of these particles shows variations in contrast in the images in Figure 15.

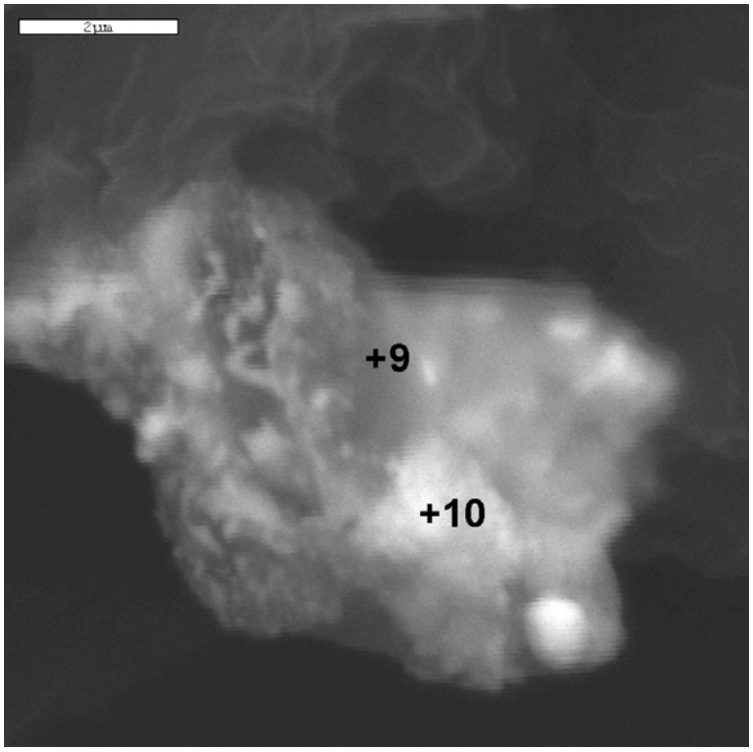

Figure 12. SEM images of a high-Pb area in Cycle 17 (Sample 11), showing approximate locations of Spectra 9 and 10 (Table 12). Faint horizontal streaking is from electrostatic charging of the sample. BSE image, scale bar: 2 μm.

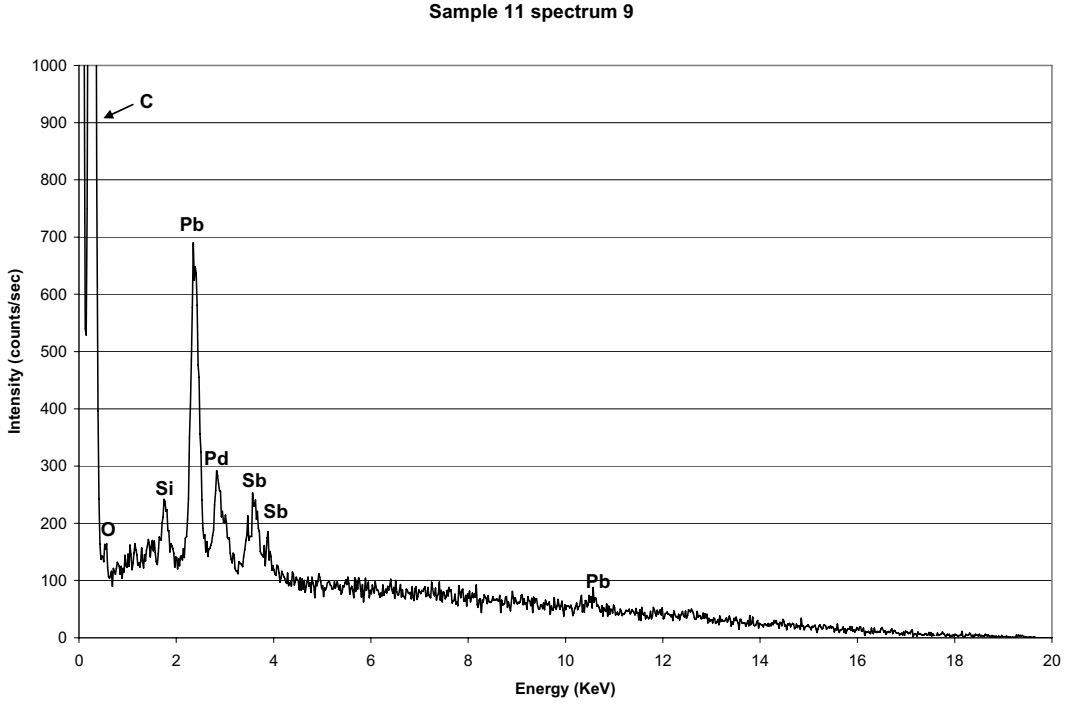

(a.)

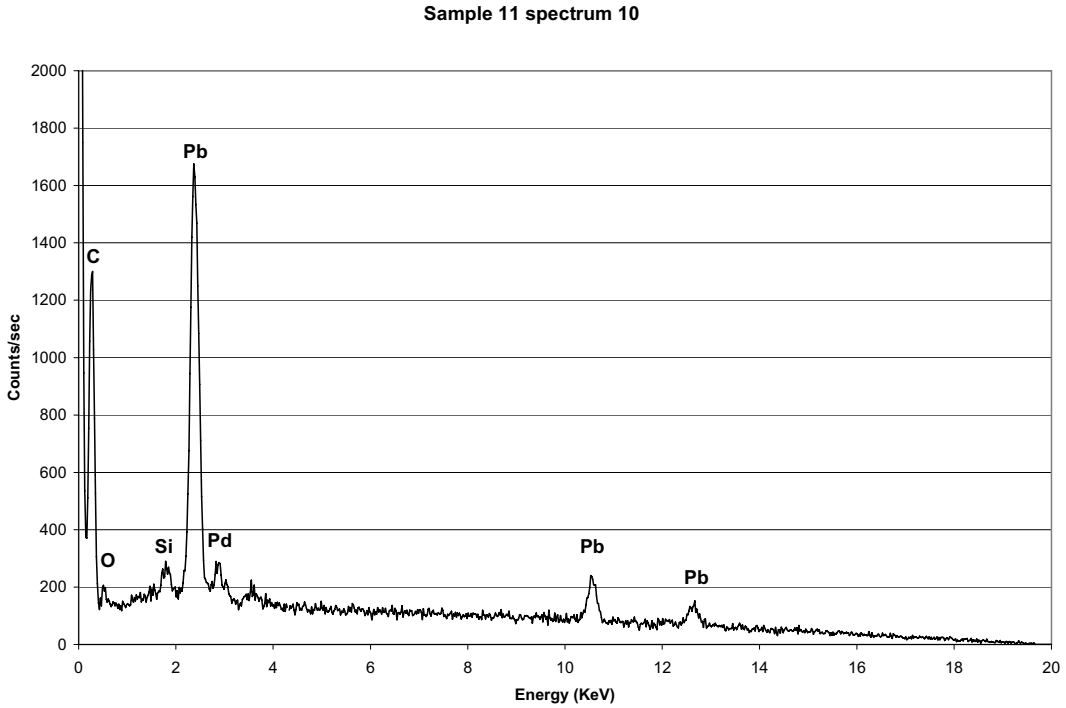

(b.)

Figure 13. EDX Spectra 9 and 10 (Cycle 17, Sample 11), showing peaks from Pb and Sb. See Table 12 for corresponding compositions. a) Spectrum 9. b) Spectrum 10.

Table 12. Atomic percentages from spectra shown in Figure 12, normalized to 100% (Cycle 17, Sample 11).

	Spectrum	
Element	9	10
Si	22.0	7.7
Sb	24.3	
Pb	53.7	92.3

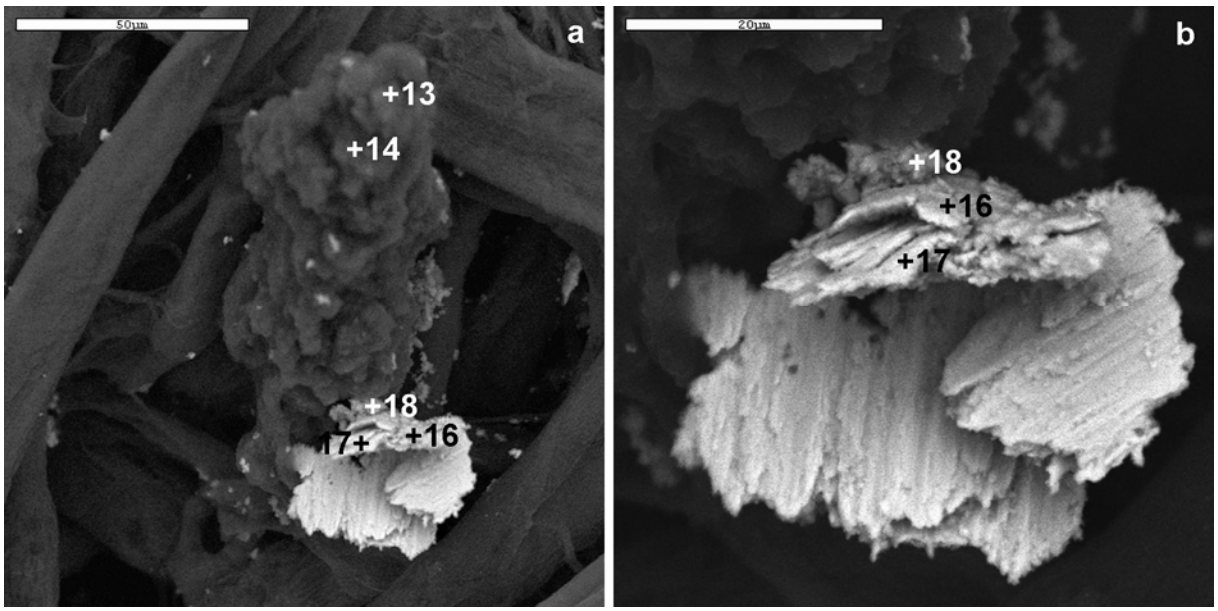

Figure 14. SEM images of an aluminosilicate material and adjacent high-Zr material, Cycle 17 (Sample 11). a) Image of entire particle both materials, with numbers showing approximate locations of Spectra 13-14 and 16-18 (Table 13). BSE image, scale bar: 50 µm. b) Higher-magnification image showing boundary between the two materials. BSE image, scale bar: 20 µm.

Table 13. Atomic percentages from SEM-EDX spectra shown in Figure 14, normalized to 100% (Cycle 17, Sample 11).

	Spectrum				
Element	13	14	16	17	18
Al	38.6	36.4			
Si	61.5	63.6			
Fe			10.9	6.6	18.6
Zr			89.1	93.4	81.4

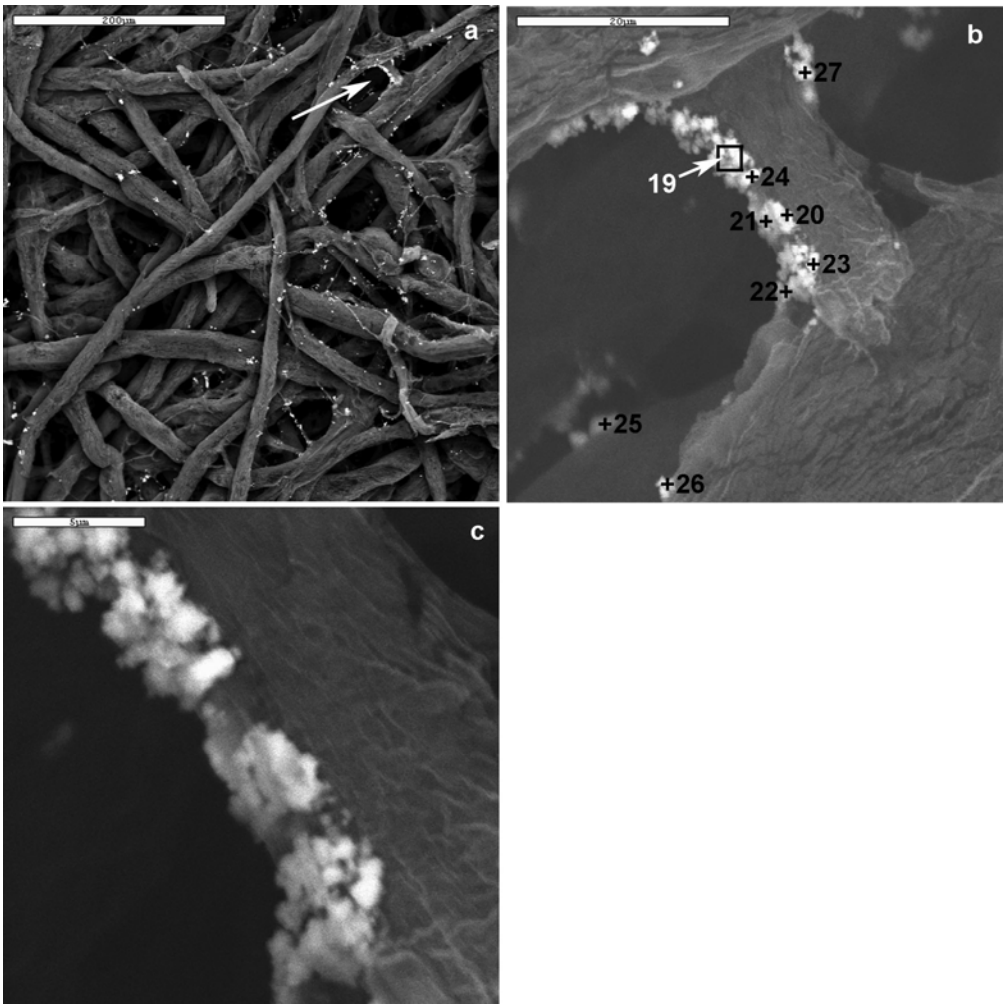

Figure 15. SEM images of numerous small particles, Cycle 17 (Sample 11). a) Low-magnification BSE image, scale bar: 200 µm. b) Higher-magnification image of area indicated by arrow in part a, showing approximate locations of Spectra 19-27 (Table 14). BSE image, scale bar: 20 µm. c) Higher-magnification image emphasizing layered structure of particles from which Spectra 19-24 were collected. Scale bar: 5 µm.

Table 14. Atomic percentages from SEM-EDX spectra shown in Figure 15, normalized to 100% (Cycle 17, Sample 11).

	Spectrum								
Element	19	20	21	22	23	24	25	26	27
Cr		2.8							
Mn		2.3							
Fe	85.5	54.4	81.5	93.5	68.2	27.3	100	14.6	74
Ni		16.9	7.0	3.5	11.4				12.3
Zn		15.1	9.0		13.6				13.8
Zr	14.5	8.5	2.5	3.0	6.8	72.7		85.46	

Figure 16 shows another area, in which two relatively large, bright particles were initially visible. Spectrum 28 (Table 15) is from the particle indicated by the arrow. The second particle, just below and slightly to the left of the tip of the arrow, jumped deeper into the filter during observation (presumably because of electrostatic charging), and thus, could not be studied in detail.

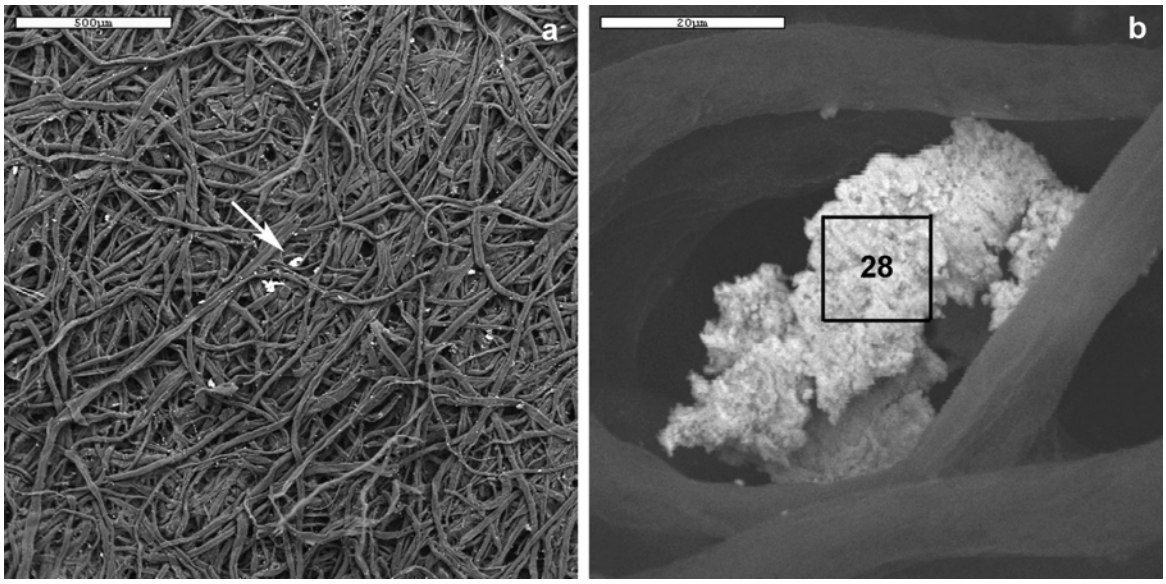

Figure 16. SEM image of a large, high-Zr particle, Cycle 17 (Sample 11). a) Low-magnification BSE image, scale bar: 500 μm. b) Higher-magnification image of particle indicated by arrow in part a, and approximate location of Spectrum 29 (Table 15). BSE image, scale bar: 20 μm.

Table 15. Atomic percentages from SEM-EDX Spectrum 28 (Figure 16), normalized to 100% (Cycle 17, Sample 11).

Element	Spectrum 28
Fe	13.6
Zr	86.4

3.2.3 Transmission electron microscopy, Sample 11 (Cycle 17)

Data from 11 particles were collected from a single TEM sample from Sample 21 (Cycle 17). Because many of the particles included more than one phase, data from each particle will be presented separately.

Figure 17 shows part of an aggregate of small, lath-shaped crystallites. EDX spectra (Table 16) show that the aggregate is primarily Fe, with significant but variable concentrations of Na, Si, and Ca. Oxygen is qualitatively present in all spectra. Because the relative proportions of Na, Si, Ca, and Fe vary widely, it is likely that the spectra represent mixtures of one or more iron oxides (including hydroxides and oxyhydroxides) with other phases containing Na, Ca, and Si.

Table 17 shows d-spacings measured from the diffraction pattern in Figure 17c, which shows numerous, highly discontinuous rings. Table 17 also shows all high-intensity d-spacings from hematite, α-Fe_2O_3. Comparison of the experimental d-spacings with those from hematite suggests that the iron oxides in the particle in Figure 17 are hematite, and that at least one other unidentified crystalline phase is

present. One possible phase might be the iron silicate hisingerite, $Fe_2Si_2O_5(OH)_4 \cdot 2H_2O$ (PDF4+ number 00-026-1140), which has high-intensity d-spacings at 0.423 and 0.246 nm.

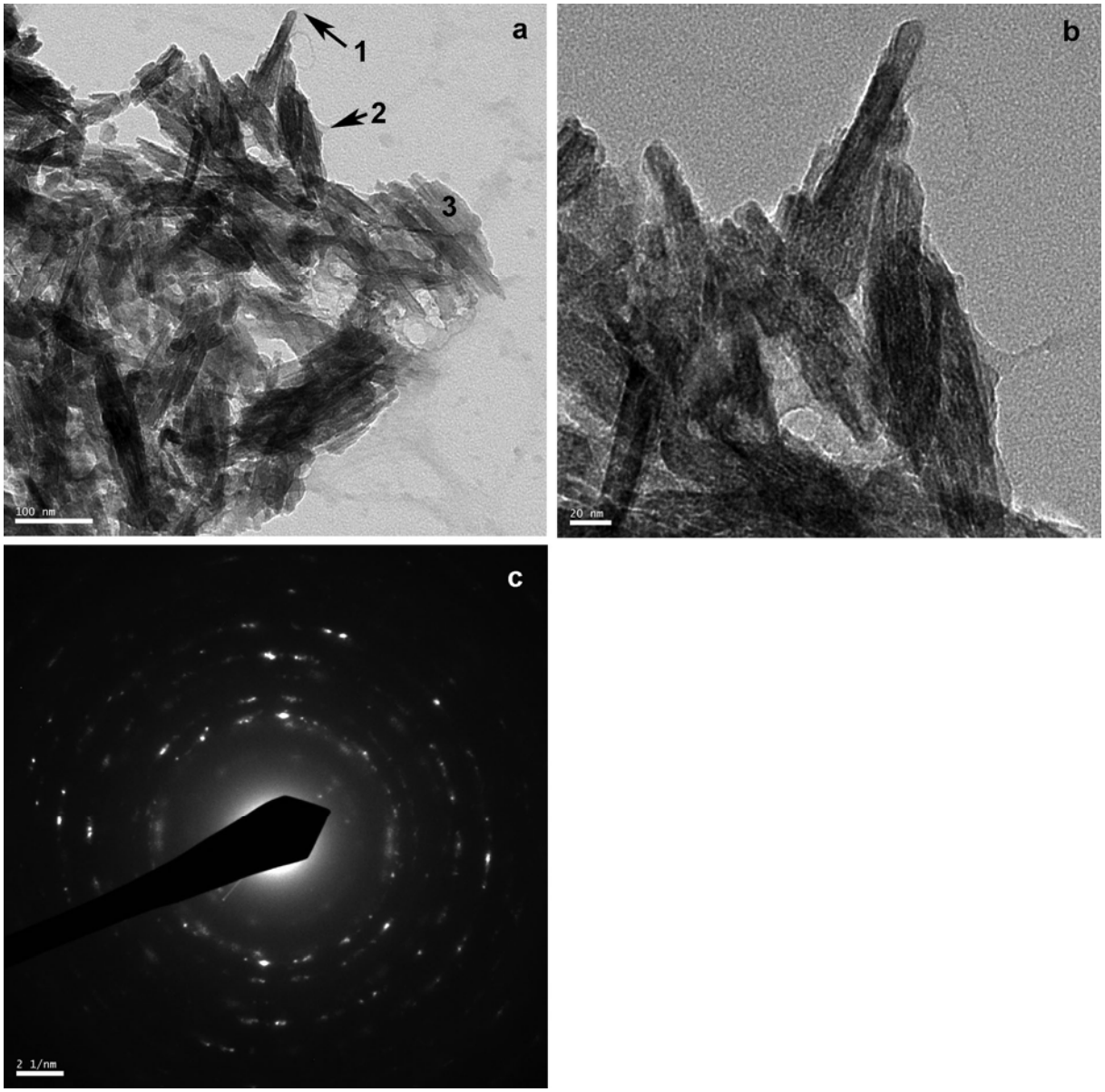

Figure 17. TEM data from a cluster of high-Fe particles, Cycle 17 (Sample 11). a) Overview of part of cluster, with numbers showing approximate locations of EDX spectra in Table 16, scale bar: 100 nm. b) Higher-magnification image of some of the crystals in part a, showing details of crystal shape and size. The mottled material in the upper right part of the figure is the carbon-coated formvar substrate used to prepare the sample. Scale bar: 20 nm. c) Diffraction pattern showing highly discontinuous rings corresponding to d-spacings in Table 17.

Table 16. Atomic percentages from TEM-EDX spectra shown in Figure 17, normalized to 100% (Cycle 17, Sample 11).

	Spectrum		
Element	1	2	3
Na		33.2	18.6
Si	15.8	4.5	13.9
Ca	20.3	1.5	8.9
Fe	63.9	60.8	58.6

Table 17. D-spacings (nm) corresponding to reflections in Figure 17c (Cycle 17, Sample 11).

Experimental	Hematite (PDF4+ No. 04-008-8479)
0.423	
0.367	0.369
0.270	0.270
0.255	0.252
0.244	
0.219	0.221
0.192	
0.186	0.184
0.172	0.172
0.145	0.145
0.140	

Figure 18 shows part of a second particle, with a large single crystal occupying most of the field of view. Table 18 contains EDX data from this crystal, indicating that it is an iron oxide, hydroxide, or oxyhydroxide. Low concentrations of other elements may either be incorporated in the crystal by solid solution or present in nearby areas of the particle. Although this crystal was not identified, its shape and size differ significantly from those of the particles in Figure 17. Shapes and sizes of synthetic iron oxides differ between phases and with differences in formation conditions.[5] Thus, it is not clear whether the particles in Figures 17 and 18 represent different phases, despite their different shapes and sizes.

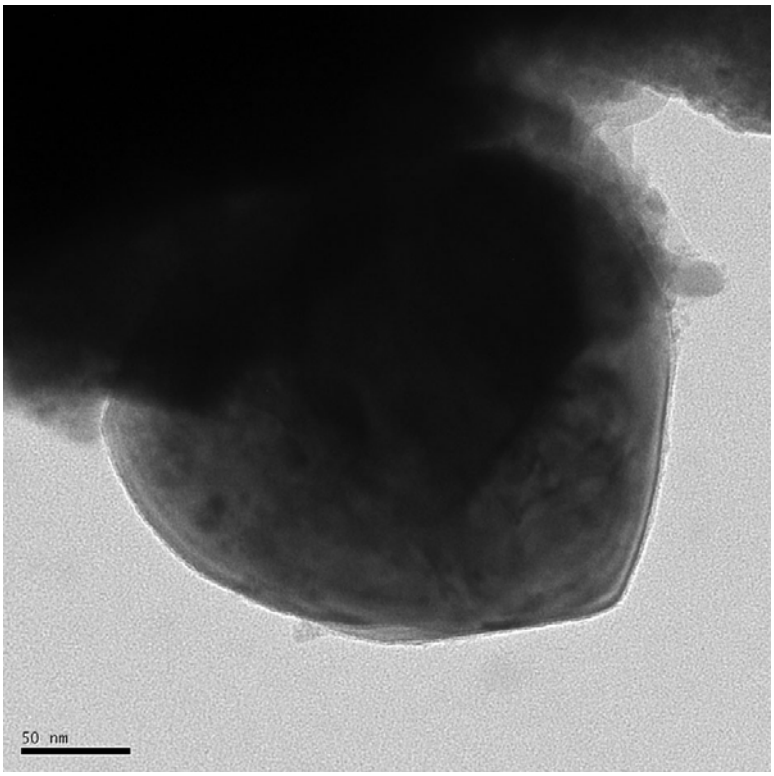

Figure 18. A single iron oxide crystal on the edge of a larger particle, Cycle 17 (Sample 11). Spectrum 4 (Table 18) is from this particle. Scale bar: 50 nm.

Table 18. Atomic percentages from TEM-EDX data from the crystal shown in Figure 18, normalized to 100% (Cycle 17, Sample 11).

Element	Spectrum 4
Si	1.6
Ca	0.7
Mn	0.9
Fe	89.7
Ni	2.4
Cu	0.7
Zn	2.9
Zr	1.2

Figures 19 and 20 show four electron-transparent areas around the edge of a large particle. EDX spectra from this particle are in Table 19. The numbers in Figures 19a and 19c shows locations of Spectra 5-11. Spectrum 12 is from the thin area in Figure 19e, Spectrum 13 is from the single crystal in the central part of Figure 20a, and Spectrum 14 is from the center of the particle, which was not electron-transparent and is not shown in any of the images. Oxygen is qualitatively present in all of the spectra, except 14.

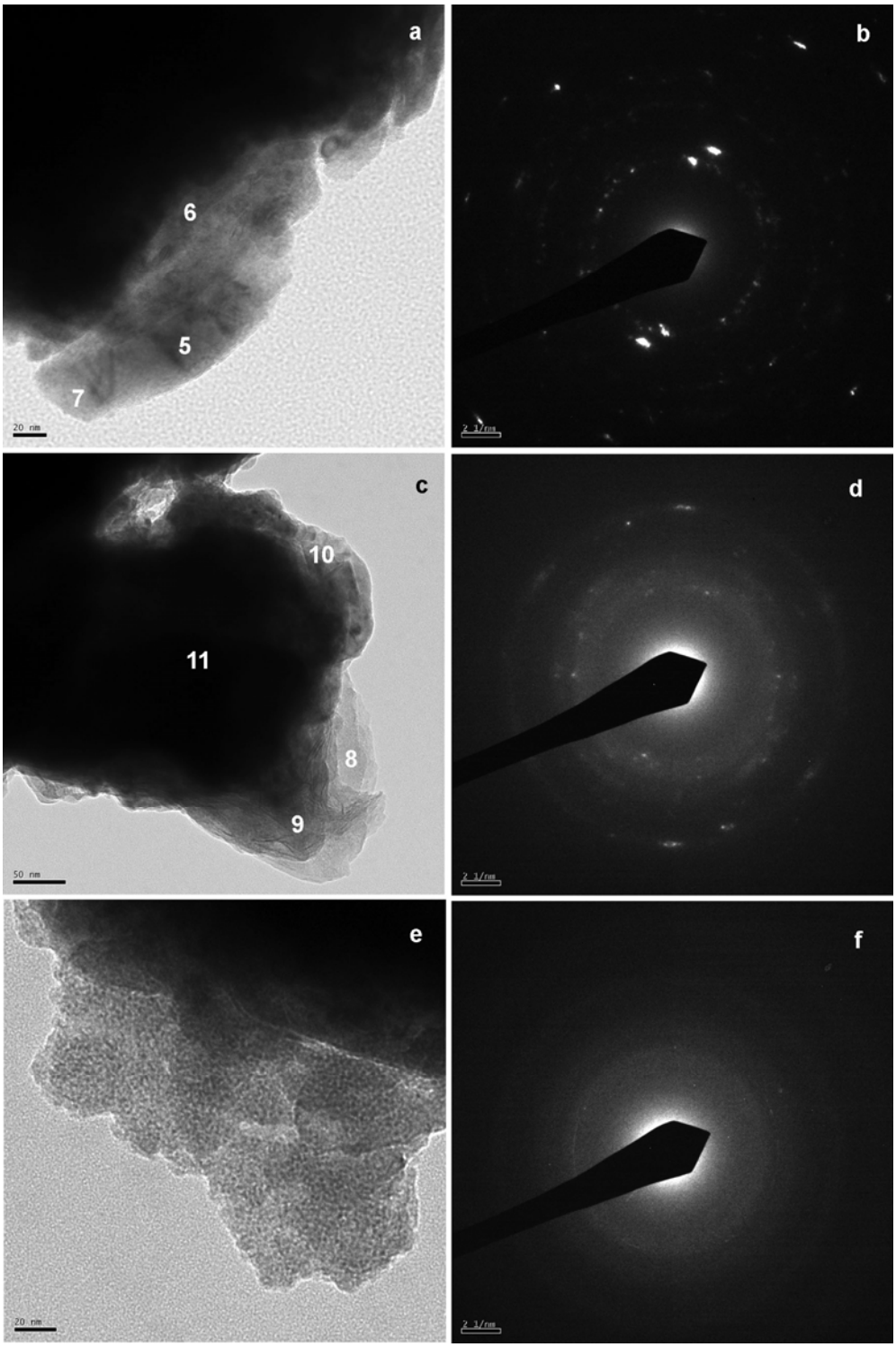

Figure 19. Three thin areas along the edge of a large particle, Cycle 17 (Sample 11). a) Image showing a thin region along the edge of the particle. Numbers indicate locations of EDX spectra in Table 19. Scale bar: 20 nm. b) Diffraction pattern corresponding to part a. c) Image showing another thin area. Numbers indicate locations of EDX spectra in Table 19. Scale bar: 50 nm. d) Diffraction pattern corresponding to part b. e) Image showing another thin area, from which Spectrum 13 (Table 19) was collected. Scale bar: 20 nm. f) Diffraction pattern corresponding to part e.

Table 19. Atomic percentages from TEM-EDX spectra shown in Figures 19 and 20, normalized to 100% (Cycle 17, Sample 11).

	Spectrum									
Element	5	6	7	8	9	10	11	12	13	14
Na				49.5	22.8	15.9			34.5	5.2
Si			2.8		5.2	3.6			4.5	3.8
Cl					2.3				4.8	
K					2.6				1.9	0.4
Ca				14.0	4.6				6.0	0.4
Mn	6.8		9.5					0.8	0.3	
Fe	43.7	8.4	52.3	28.2	29.9	23.9	25.2	96.4	42.4	14.0
Ni	10.9		11.9			6.2	0.6	0.4	0.1	
Cu	2.7	1.2	5.3		0.7		2.6			
Zn	14.2		13.1	3.6	1.2	5.0	6.9		2.4	1.2
Zr	21.6	90.4	5.1	4.6	30.9	45.4	64.7	2.3	2.4	75.0
Pb									0.6	

Figure 19a shows an elongated electron-transparent area along the edge of the particle. The black area in the upper left of the figure was not electron transparent, and is therefore, probably not represented in the diffraction pattern (Figure 19b). Spectra 5 and 7 are from the thin areas, and appear to represent iron oxides with Mn, Ni, Cu, and Zn. Spectrum 6 was collected adjacent to the thick material, and suggests that this material is probably part of the cladding. The Zr in Spectra 5 and 7 probably represents characteristic x-rays generated in this material.

The diffraction pattern in Figure 19b shows numerous faint individual reflections and highly discontinuous rings. Because of the faintness of the reflections and absence of either clear rings or a single-crystal lattice pattern, it is difficult to measure d-spacings accurately. Thus, the pattern may include many d-spacings that were not measured. Nonetheless, the diffraction pattern shows d-spacings of approximately 0.169, 0.183, 0.252, 0.274, 0.295, and 0.364 nm. As Table 17 shows, all of these d-spacings except that of 0.295 nm correspond to high-intensity d-spacings of hematite, assuming that measurement errors are slightly larger than normal.

Hematite with 9% Cu has been synthesized in the laboratory, as have hematite crystals coated with silica, Cr hydroxide, Zr oxide, or Mn hydroxide[5]. Nonetheless, the 0.295 nm d-spacing and presence of significant concentrations of Mn, Ni, and Zn both suggest that the area of the sample represented by the diffraction pattern may contain one or more spinel phases in addition to the hematite. Possibilities include magnetite (Fe_3O_4), jacobsite ($MnFe_2O_4$), trevorite ($NiFe_2O_4$), franklinite ($ZnFe_2O_4$), or a solid solution between these minerals.

Figure 19c shows another thin region along the edge of the same particle. Numbers indicate locations of Spectra 8-11 (Table 19). The fraction of Zr increases closer to the thick area sampled by Spectrum 11, suggesting that the Zr in Spectra 8-10 may be at least in part from unintentional incorporation of characteristic x-rays from thicker parts of the sample. The significant concentrations of Na and Ca, and measurable concentrations of Si, Cl, and K, are unusual in the crud samples considered in

this paper. The area from which Spectrum 9 was collected has a wispy, somewhat wrinkled appearance that is also unusual.

The diffraction pattern from this area (Figure 19d) shows three broad, diffuse, continuous rings and several faint, diffuse, reflections. One of the rings extends with nearly constant intensity between d-spacings of approximately 0.24 and 0.31 nm. The second ring corresponds to a d-spacing of approximately 0.21 nm, and the third to a d-spacing of approximately 0.15 nm. This information is not sufficient to allow phase identification.

Although attempts to divide the elements present between various phases are necessarily speculative, it seems possible that this are contains three distinct phases, possibly in layers approximately parallel to the sample substrate. One phase is very high in Zr, and may be the cladding. A second phase contains the Na, Si, Cl, K, and Ca. The third phase may be an iron oxide.

Figure 19e shows another thin region along the edge of the same large particle. Spectrum 13 was collected from the thin material. The diffraction pattern shows three very faint, diffuse, continuous rings corresponding to d-spacings of approximately 0.15, 0.20, and 0.27 nm. Although Spectrum 9 has a higher concentration of Zr than Spectrum 13 (perhaps because it was collected closer to the thick, high-Zr materials), the two spectra appear to represent the same material.

Figure 20 shows an individual crystal at the edge of the same large particle as the data in Figure 19, and a single-crystal diffraction pattern. The diffraction pattern (Figure 20b) is consistent with hematite (α-Fe_2O_3), and could not have been produced by magnetite (Fe_3O_4), goethite (α -FeOOH), or lepidocrocite (γ-FeOOH).

Figure 21 shows another small particle, which consists of a single crystal (large dark area in the left part of the particle in Figure 21a) and a cluster of smaller crystallites (right part of the particle). The corresponding EDX Spectra (15 and 16) show large peaks from Pb, Au, Fe, and Cobalt (Co). Gold peaks are present in all of the TEM-EDX spectra in this study, and are assumed to be from the Au grid used to support the particles. These peaks are unusually large relative to those from the sample itself, probably in part because the particle was close to a grid bar and because the Pb may have been unusually effective at scattering electrons from the beam into adjacent materials. Fe and Co are also probably artifacts, produced when the sample scattered electrons into the pole piece of the microscope, exciting Fe and Co characteristic x-rays.

As discussed in the section on SEM analyses, determining concentrations of Pb from EDX data is complicated by two series of possible peak overlaps: one between approximately 1.5 to 2.7 keV (primarily involving the Pb Mα, S Kα, and Mo Lα x-rays) and the other between approximately 10.4 and 10.7 keV (involving the Pb Lα and As Kα x-rays). Successfully interpreting x-rays involved in these overlaps requires careful qualitative analysis of all peaks in the entire spectrum, followed by selection of appropriate peaks for quantification.

Table 21 shows all x-rays with high relative intensities between 1.5 and 2.7 or 10.4 and 10.7 keV. Most of the possible elements (including Mo) can be eliminated because their presence in significant concentrations would imply the presence of other peaks that do not appear in the experimental spectra. Pb was identified based on the presence of the Pb Lα, Pb Lβ, and Pb Lγ x-rays; however, the presence of significant concentrations of S (in addition to the Pb) cannot be ruled out. As noted in Table 21, small peaks (corresponding to low concentrations) from Rb, Si, W, and P may also be present, but cannot be qualitatively distinguished from the large peaks with similar energies from elements known to be present. Thus, this particle is interpreted as representing essentially pure Pb (possibly with light elements).

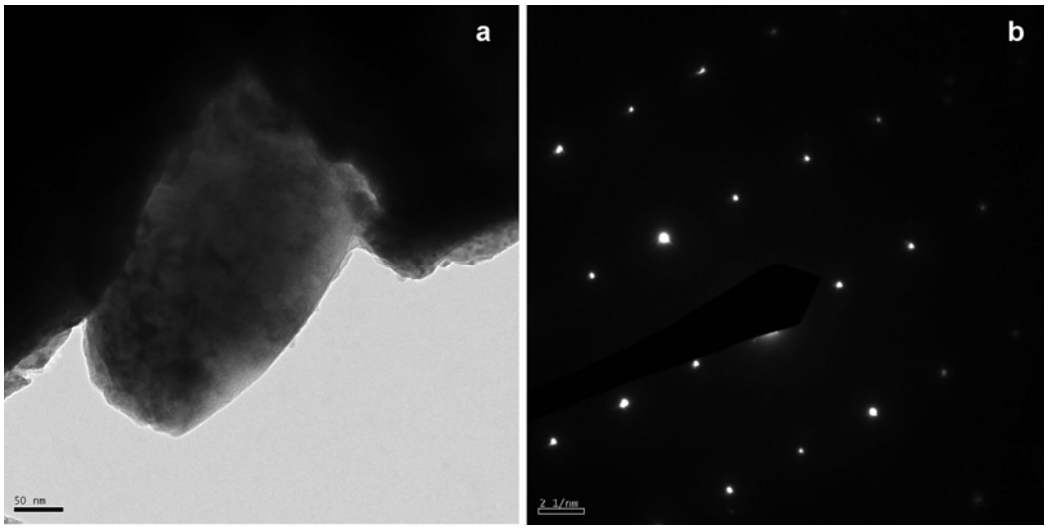

Figure 20. A single electron-transparent crystal along the edge of the large particle shown in Figure 19, Cycle 17 (Sample 11). Spectrum 12 (Table 19) was collected from this crystal. a) Image, scale bar: 50 nm. b) Single-crystal diffraction pattern (hematite, beam approximately parallel to <5 4 -2>).

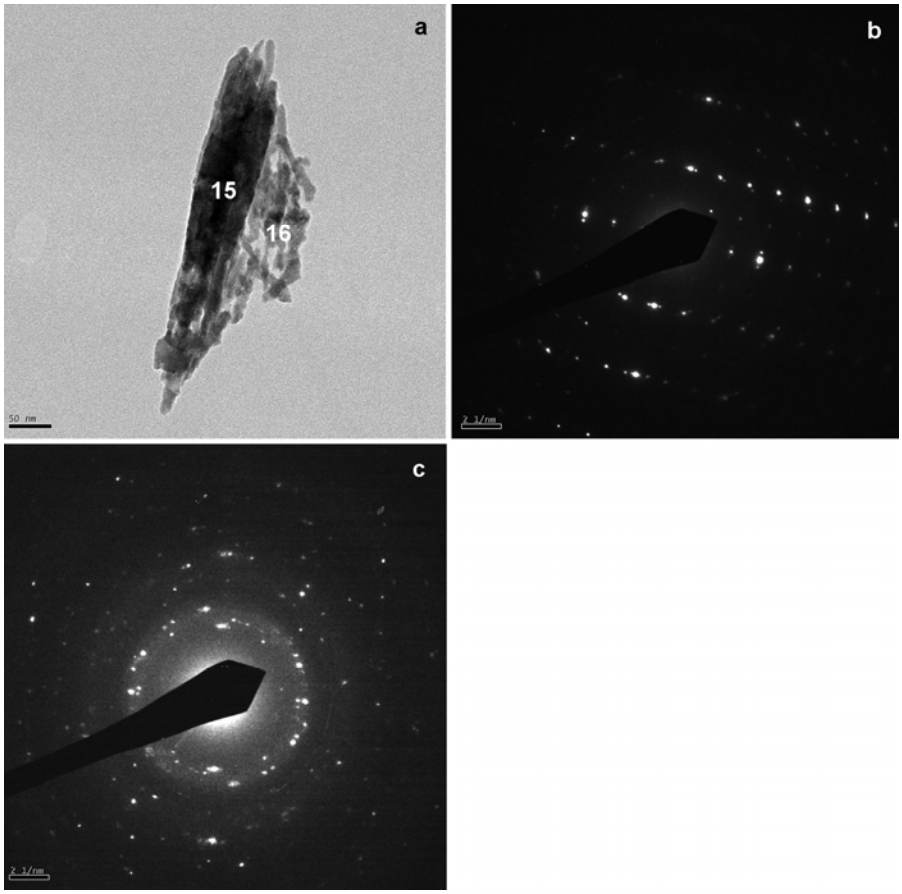

Figure 21. A small high-Pb particle, Cycle 17 (Sample 11). a) Image of entire particle. Numbers indicate locations of EDX spectra in Table 20. Scale bar: 50 nm. b) Diffraction pattern from dark area in which Spectrum 15 was collected. c) Diffraction pattern from group of small particles from which Spectrum 16 was collected.

Table 21. Characteristic x-rays with high relative intensities that have possible peak overlaps with Pb[4].

X-ray	Energy (keV)	Relative Intensity	Present in spectrum?	Comments
Lu $M\alpha_1$	1.581	100	No	No La1
Kr $L_{1,2}$	1.586	111	No	Unlikely in high vacuum
Hf $M\alpha_1$	1.645	100	No	No La1
Rb $L\alpha_1$	1.694	100	?	
Ta $M\alpha_1$	1.710	100	No	No La1
Si $K\alpha$	1.740	100	?	Common in other areas of specimen
W $M\alpha_1$	1.775	100	?	Possible instrument artifact?
Sr $L\alpha_1$	1.807	100	No	No Ka1
Re $M\alpha_1$	1.843	100	No	No La1
Os $M\alpha_1$	1.910	100	No	No La1
Y $L\alpha_1$	1.923	100	No	No Ka1
Ir $M\alpha_1$	1.980	100	No	No La1
P $K\alpha$	2.013	100	?	
Zr $L\alpha$	2.040	100	No	No Ka1
Pt $M\alpha_1$	2.051	100	No	No La1
Au $M\alpha_1$	2.123	100	Yes	From grid
Nb $L\alpha$	2.166	100	No	No Ka1
Hg $M\alpha_1$	2.196	100	No	No La1
Tl $M\alpha_1$	2.271	100	No	No La1
Mo $L\alpha$	2.290	100	No	No Ka1
S $K\alpha$	2.308	100	?	
Pb $M\alpha_1$	2.346	100	Yes	L-series present
As $K\alpha$	10.544	100	No	No Kb
Pb $L\alpha_1$	10.552	100	Yes	Other L-series peaks present

The diffraction data were not analyzed in detail because the composition makes it likely that this particle is not part of the crud deposits forming on the surface of the fuel pin.

Figure 22 shows another small particle, which appears to consist of numerous overlapping layers. EDX Spectra 17, 18, and 19 (Table 22) were collected from relatively thin areas around the edges of the particle, and represent essentially pure Zr or Fe (possibly including oxides, hydroxides, etc.). Spectrum 20 was collected from the thicker, central, part of the particle, and shows small concentrations of Ni and Cu in addition to Zr and Fe.

Figure 22b (a diffraction pattern from the entire particle) shows numerous discontinuous rings and individual reflections. The largest d-spacing represented is approximately 0.357 nm, which does not correspond to a high-intensity d-spacing from any iron oxide or hydroxide. The absence of reflections from larger d-spacings probably indicates that either the iron oxide has a strong preferred orientation or it is not diffracting strongly enough to produce readily visible reflections. In either case, identifying it based only on reflections that do not overlap those produced by the high-Zr phase is prohibitively difficult.

This particle appears to be a small fragment of cladding with the immediately adjacent high-iron crud. Unfortunately (but not surprisingly, given the sample-preparation technique), the fragment is apparently lying flat on the substrate, with the interface between the cladding and the crud approximately perpendicular to the electron beam. Thus, little information can be obtained about possible structural or compositional differences in layers parallel to the surface of the cladding.

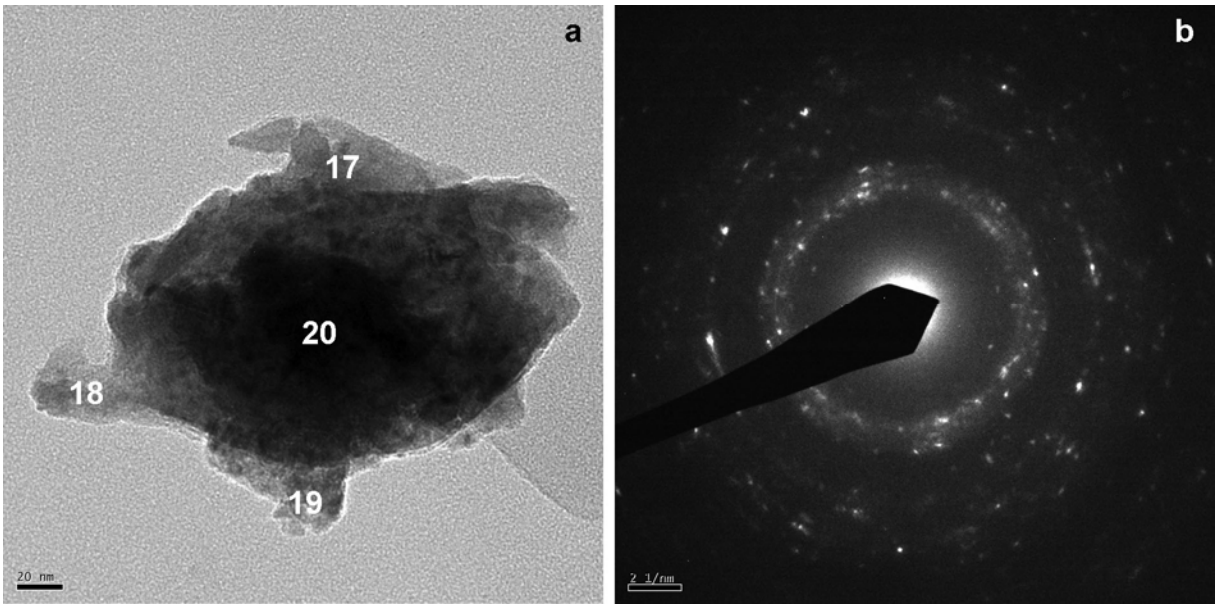

Figure 22. A small particle with high-Zr and high-Fe areas, Cycle 17 (Sample 11). a) Image of particle. Numbers indicate locations of EDX spectra in Table 22. Scale bar: 20 nm. b) Diffraction pattern from entire particle.

Table 22. Atomic percentages from TEM-EDX spectra shown in Figure 22, normalized to 100% (Cycle 17, Sample 11).

	Spectrum			
Element	17	18	19	20
Fe			100	14.5
Ni				0.3
Cu				0.6
Zr	100	100		84.6

Figure 23 shows a relatively large particle, which apparently consists of a single large crystal with numerous smaller crystals and an area of wispy material on its outer surface. Dark areas such as that indicated by the arrow may indicate either smaller crystals on the upper or lower surface of the large crystal or regions of different composition or orientation inside the large crystal. Table 23 shows compositions from this particle: Spectrum 21 is from the wispy material, Spectrum 24 is from one of the small surface crystals, and Spectrum 23 is from the large crystal itself. Spectra 21 and 24 probably both included characteristic x-rays from the adjacent large crystal.

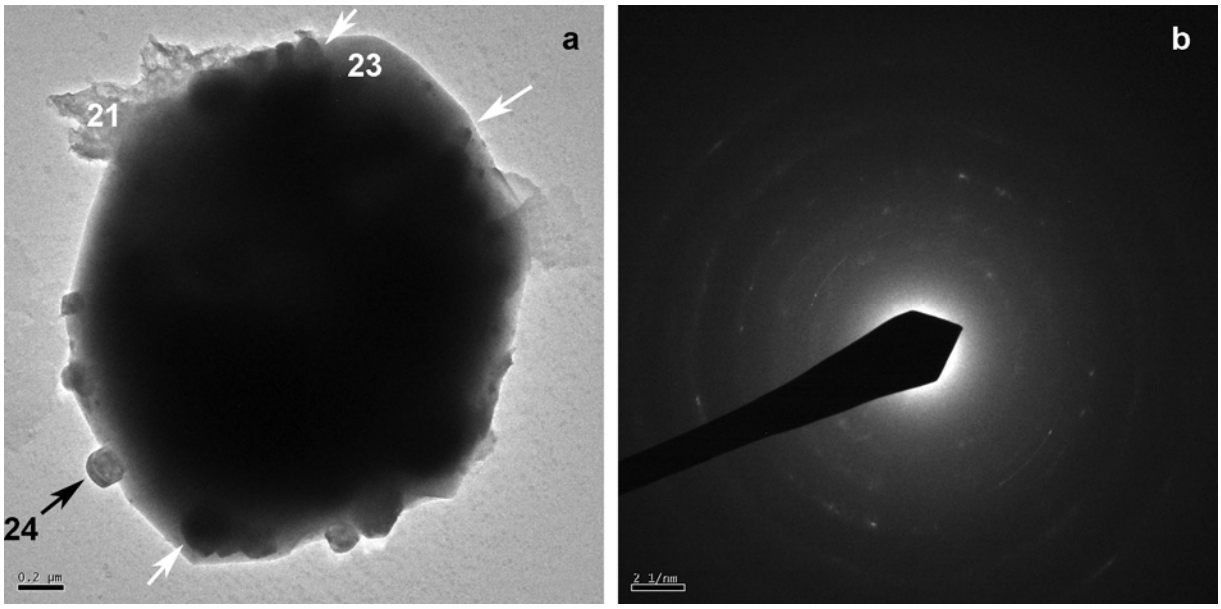

Figure 23. A particle consisting of a large crystal and numerous smaller ones, Cycle 17 (Sample 11).
a) Image of particle. Numbers indicate locations of EDX spectra in Table 23. White arrows show boundaries of dark areas inside the perimeter of the large crystal, which may be either small crystals on its upper or lower surfaces or inclusions with different compositions or orientations. Scale bar: 200 nm.
b) Diffraction pattern from area including Spectrum 21.

Table 23. Atomic percentages from TEM-EDX spectra shown in Figure 23, normalized to 100%. (Cycle 17, Sample 11)

	Spectrum		
Element	21	23	24
Si	3.3		
Cl	3.0		
K	1.4		
Ca	4.9		
Fe	81.2	100	100
Cu	1.4		
Zn	4.6		
Pb	0.4		

The EDX spectra indicate that the large particle and small particle are both iron oxides, hydroxides, or oxyhydroxides. EDX data from the wispy material show that it contains low concentrations of Si, Cl, K, Ca, Cu, and Zn, in addition to Fe (which may however, include characteristic x-rays from the adjacent large particle).

No diffraction data were collected from the large particle. When contrast is appropriately adjusted, the diffraction pattern from the wispy material (Figure 23b) shows very faint, diffuse, continuous rings corresponding to d-spacings of approximately 0.121, 0.140, 0.153, 0.193, 0.235, and 0.331 nm. Because

of the faintness of the rings (which is probably due in part to the very small volume of material involved), it is difficult to be certain that all d-spacings with significant diffracted intensity have been included. Nonetheless, these d-spacings are consistent with an identification of lepidocrocite, γ-FeOOH, assuming a preferred orientation in which crystallites are lying on their (010) faces (in space group *Amam*) and an otherwise random orientation, and are not consistent with any other iron oxide, hydroxide, or oxyhydroxide in the PDF4+ database.

Figure 24 shows a complex particle, with numerous bright and dark areas. The EDX spectra (Table 24) differ significantly from those in other particles, and contain the only high concentrations of Al, Cr, and Zn reported in this study. The high concentrations of Na are likewise unusual from material that appears crystalline in TEM images.

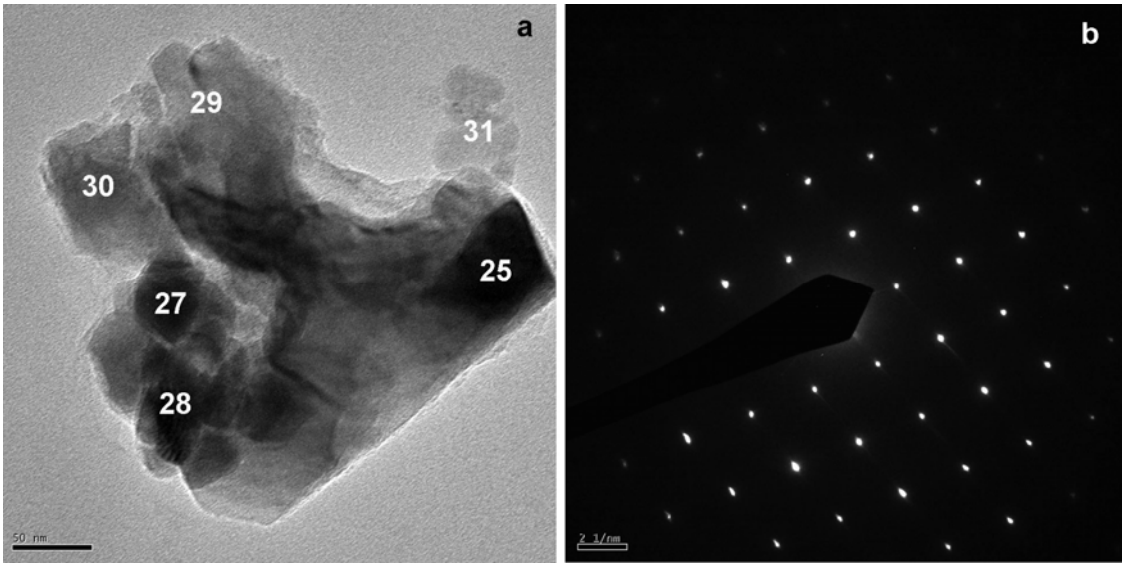

Figure 24. A complex particle with numerous dark and light domains, some of which have high concentrations of Na, Al, Cr, or Zn, Cycle 17 (Sample 11). a) Image of particle. Numbers indicate locations of EDX spectra in Table 24. Scale bar: 50 nm. b) Diffraction pattern from area including Spectrum 25.

Table 24. Atomic percentages from TEM-EDX spectra shown in Figure 24, normalized to 100% (Cycle 17, Sample 11).

	Spectrum					
Element	25	27	28	29	30	31
Na K	22.7		16.5	18.8	20.8	
Al K	36.2	13.6	18.3	17.9	37.9	8.62
Si K	3.5	13.4	4.6	9.9	10.2	3.49
Ca K		1.7	0.5			
Cr K	9.7	1.1	3.5	25.7	5.6	16.74
Fe K						47.66
Ni K	1.6	0.5	1.2	1.6	1.9	19.59
Cu K	0.5	1.3	1.0	0.7	0.8	
Zn K	25.8	9.6	13.5	25.4	22.8	3.90
Zr L		58.9	40.9			

Because of the small sizes of the domains of different contrast, it was extremely difficult to tilt the particle into different orientations to obtain patterns from each area. Thus, there is only one single-crystal diffraction pattern (Figure 24b, which corresponds to Spectrum 25). The composition of this crystal might represent numerous minerals or combinations of minerals, making it prohibitively difficult to compile a list of candidate phases to be compared to the diffraction pattern. Thus, the phase represented by the data was not identified.

Figure 25 shows a complex particle consisting of numerous round domains, some only approximately 10 nm across. The EDX spectra (Table 25) indicate that the particle is an iron oxide, hydroxide, or oxyhydroxide, with significant concentrations of Na, Si, and Zn. The diffraction pattern (Figure 25b) shows numerous individual reflections, some of which form a highly discontinuous ring corresponding to a d-spacing of 0.254 nm. Other d-spacings represented in the pattern include 0.146, 0.158, 0.170, 0.210, 0.297, and 0.479 nm. All of these d-spacings are consistent with magnetite (Fe_3O_4), but not with hematite, lepidocrocite, or goethite.

Figure 26 shows another complex particle, which contains several areas with straight edges that appear very dark in the figure and a larger, lighter colored area with irregular boundaries. The EDX data (Table 26) show that Spectra 36 and 38 (both from dark areas) are iron oxides, hydroxides, or oxyhydroxides. Figure 26c (a single-crystal diffraction pattern from the same crystal as Spectrum 36) shows the same d-spacings and interplanar angles as Figure 20b, and therefore, it is identified as hematite.

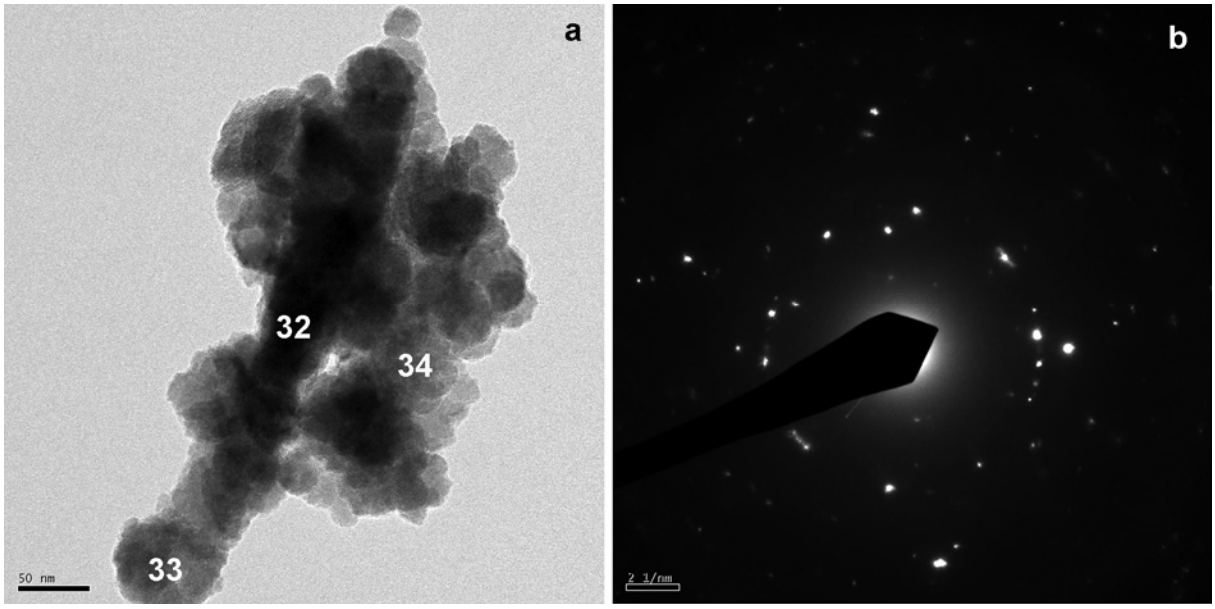

Figure 25. A complex particle with numerous domains, some as small as 10 nm across, Cycle 17 (Sample 11). a) Image of particle. Numbers indicate locations of EDX spectra in Table 25. Scale bar: 50 nm. b) Diffraction pattern from entire particle.

Table 25. Atomic percentages from TEM-EDX spectra shown in Figure 25, normalized to 100% (Cycle 17, Sample 11).

	Spectrum		
Element	32	33	34
Na	5.8	13.4	10.6
Si	3.5	4.2	5.0
Fe	87.5	77.1	79.7
Zn	3.2	5.4	4.7

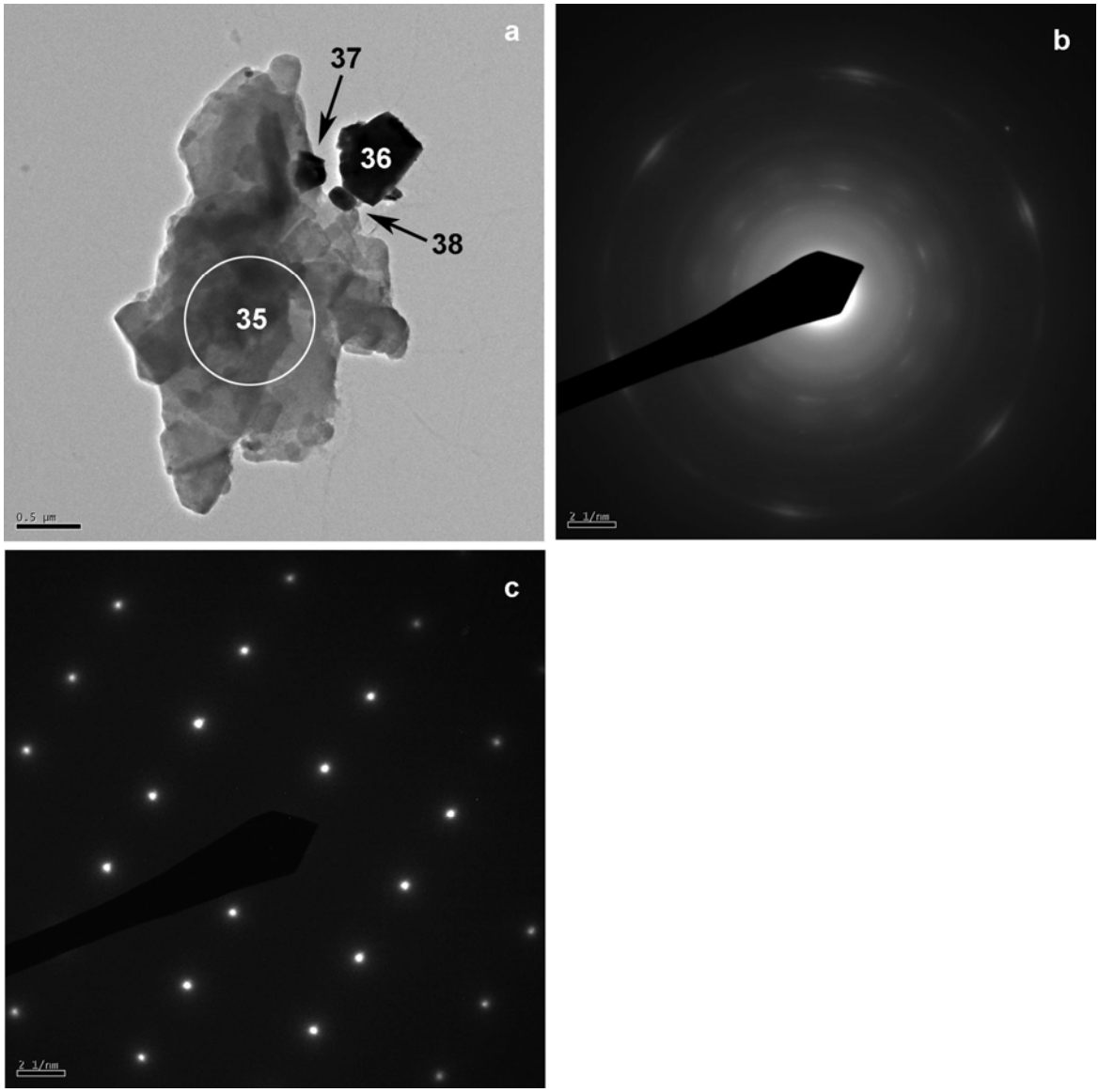

Figure 26. A complex particle containing Fe oxides, Fe-Zr phases, and aluminosilicates, Cycle 17 (Sample 11). a) Image of particle. Numbers indicate locations of EDX spectra in Table 26. The circle indicates the approximate area included in Spectrum 35. Scale bar: 500 nm. b) Diffraction pattern from approximate area shown by circle in part a. c) Diffraction pattern from crystal with Spectrum 36.

Table 26: Atomic percentages from TEM-EDX spectra shown in Figure 26, normalized to 100% (Cycle 17, Sample 11).

	Spectrum			
Element	35	36	37	38
Na	3.1	2		
Al	46.8			1.6
Si	42.3	1.6	3.8	
Cl	0.9			
K	0.4			
Ca	0.3			
Ti	0.3			
Mn			2.8	
Fe	0.9	96.3	64.6	98.4
Ni			6.4	
Cu			5.6	
Zn			16.8	

Spectrum 37 (also from a dark area) contains significant concentrations of Zn and smaller concentrations of Si, Ni, and Cu, in addition to the Fe. If the EDX data are taken at face value, the Zn:Fe ratio is approximately 1:4, indicating that the particle cannot be franklinite ($ZnFe_2O_4$, a spinel identified in TEM analyses of other crud samples[1]). However, it is possible that some of the Fe in the spectrum is from characteristic x-rays from the adjacent Fe oxides, in which case, the actual Zn:Fe ratio of the Zn-bearing phase would be lower. No diffraction data were collected from this phase.

Spectrum 35 apparently represents an aluminosilicate with an Al:Si ratio of approximately 1:1, and perhaps with a low concentration of Na. The corresponding diffraction pattern (Figure 26b) shows rings corresponding to d-spacings of approximately 0.138, 0.144, 0.201, 0.247, 0.289, and 0.349 nm. Large variations in intensity around each ring suggest a strong preferred orientation, and the image suggests that this material may consist of numerous overlapping plates, each approximately parallel to the substrate. The chemical data suggest that this material might be kaolinite, halloysite, metahalloysite, dickite, nacrite, or beidellite. (Kaolinite, halloysite, metahalloysite, dickite, and nacrite are all $Al_2Si_2O_5(OH)_4$, some of these phases also include water; beidellite is chemically similar, but has low concentrations of Na or Ca.) However, the measured d-spacings do not match those for any of these minerals in the PDF4+ database. It is not clear whether this lack of correspondence between the experimental data and the database is because the material in the sample has a preferred orientation, or whether it represents another phase entirely.

Figure 27 shows another particle, which apparently consists of domains ~10 nm across. The EDX data (Table 27) show large concentrations of Na and Si, a significant concentration of Cl, and low concentrations of Al, K, and Ca. The diffraction pattern (Figure 28b) shows two obvious rings corresponding to d-spacings of 0.202 and 0.282 nm and a very faint ring corresponding to a d-spacing of 0.329 nm. These d-spacings do not match any pattern for a material containing only Na, Si, Al, Cl, K, Ca, O, and elements lighter than C in the PDF4+ database. However, they are a close match to the d-spacings expected from NaCl (halite), suggesting that the particle may be a mixture of halite and amorphous silica.

As noted in similar patterns observed by Janney and Porter[1], concentrations of Na are higher than would be expected from NaCl alone, and it is possible that another Na-bearing phase not identified in the diffraction data may be present.

Figure 28 shows another particle, which consists of several large crystalline domains. The EDX data (Table 28) indicates that the particle is an iron oxide, with low concentrations of Cr, Mn, Ni, and Cu. Although the EDX spectrum shows a small peak from Co, it is likely that this peak is an artifact. The Na and Si may indicate that the wispy material in the extreme upper left of the image overlaps the particle in the area of the EDX spectrum. No diffraction data was collected, and the specific phase shown here was not identified.

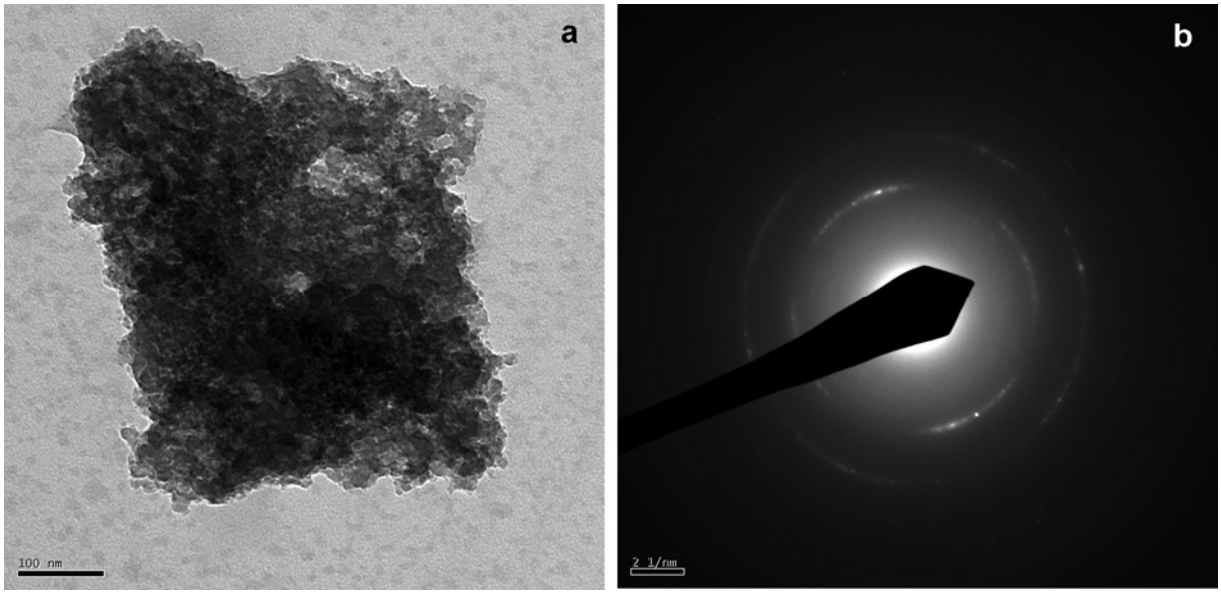

Figure 27. Particle from which Spectrum 39 (Table 27) was collected, Cycle 17 (Sample 11) a) Image of particle. Scale bar: 100 nm. b) Diffraction pattern from entire particle.

Table 27. Atomic percentages from the TEM-EDX spectrum shown in Figure 27, normalized to 100% (Cycle 17, Sample 11).

Element	Spectrum 39
Na	36.5
Al	3.6
Si	41.9
Cl	11.9
K	2.0
Ca	4.1

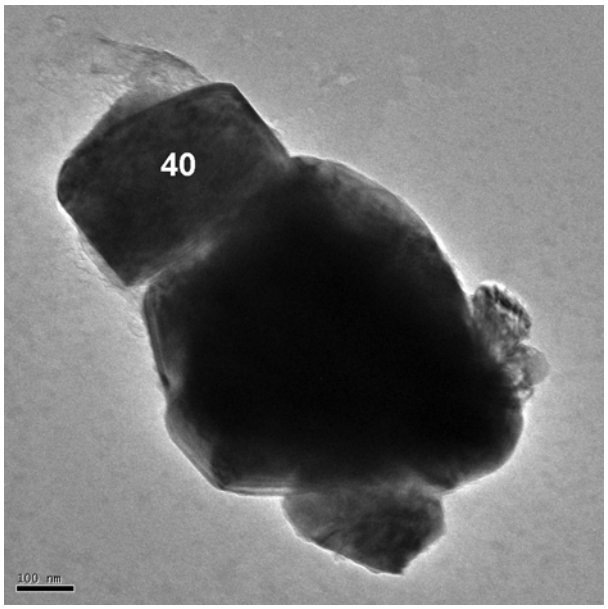

Figure 28: Image of Particle from which Spectrum 40 (Table 28) was collected, Cycle 17 (Sample 11), scale bar: 100 nm.

Table 28. Atomic percentages from the TEM-EDX spectrum shown in Figure 28, normalized to 100% (Cycle 17, Sample 11).

Element	Spectrum 40
Na	2.8
Si	1.5
Cr	0.8
Mn	0.3
Fe	92.1
Co	2.0
Ni	0.4
Cu	0.2

3.2.4 Analytical Laboratory Results, Cycle 17

Elemental concentrations from Cycle 17 samples are reported in Appendix H, together with the composition of a filter paper similar to that used to collect Samples 10 and 11. Concentrations of K, Ni, Sr, and Zn are higher in the filter paper than in either of the samples, and concentrations of Cr and Mn are higher in the filter paper than in one of the samples. These relationships suggest that the filter paper is not an appropriate "blank" for Samples 10 and 11. Concentrations of Zr are much higher in both samples than in the filter paper, and probably represent cladding fragments in the samples.

Optical observations of Sample 12 suggest that it contains little or no crud. Thus, the analyses presented in Appendix H probably represent the wire mesh used to collect the sample rather than any characteristics of the crud itself.

4. DISCUSSION

Few of the crud particles in Sample 21 (cycle 16) are large enough to be distinguished as individuals in optical micrographs. SEM data suggest that many particles are at most a micrometer or two across. Many SEM-EDX spectra from relatively large (few micrometers to few tens of micrometers) particles show only Al, many consist primarily of Zr, and a much smaller number consist primarily of Fe. Lower concentrations of other elements may indicate that the spectra include characteristic x-rays from more than one particle (especially Spectrum 40, which is from a relatively large area).

The TEM data from Sample 21 are consistent with the SEM data in that they confirm the presence of high-Al particles (identified from diffraction data as corundum, α-Al_2O_3), high-Zr particles (not analyzed in detail, as they were believed to be fragments of cladding rather than crud), and high-Fe particles (all identified as hematite, α-Fe_2O_3). However, the TEM data also show two phases not represented in the SEM data: a beam-sensitive aluminosilicate with several times as much Si as Al and with some Na, Ca, and Sr, and a high-Na phase that also contains Cl. The aluminosilicate is probably a clay mineral; however, neither phase could be conclusively identified.

None of the SEM images from Sample 21 show particles that appear to include more than one phase. All but one of the particles studied with TEM consists of numerous smaller pieces; however, it is not clear whether these pieces were adjacent to one another in the original crud or whether they became agglomerated during sample preparation. The TEM-EDX analyses showing numerous elements whose proportions vary widely from place to place in the same particle suggest that more than one phase is present, possibly in separate small pieces.

In contrast, no high-Al particles comparable to those in Sample 21 were observed in SEM data from Sample 11 (Cycle 17). Many particles contain more than one phase. Although most individual particles are too small for detailed analysis, several contain distinct high-Fe and high-Zr regions, and small areas of high-Zr material are attached to or embedded in lumpy particles with an Al:Si ratio of approximately 1:2. One small area of Pb was observed in this sample.

TEM data from Sample 11 (Cycle 17) show numerous examples of hematite, with wide variation in crystal sizes and shapes. Other data suggest the presence of magnetite (Fe_3O_4), lepidocrocite (γ-FeOOH), and a clay with an aluminum:silicon ratio of approximately 1:1. One high-Pb particle was also observed in this sample. Many areas are nanocrystalline, and the diffraction data indicate other unidentified phases in the particles in this paper.

If materials with high concentrations of Zr are interpreted as pieces of cladding, the SEM data from Sample 11 includes particles that contain the interface between the cladding and the immediately adjacent crud. TEM data from the particles represented in Figures 19, 20, and 23 shows that the central parts of these particles are high in Zr and too thick to be electron transparent, while electron-transparent areas around the edges are high in Fe. Unfortunately, but not surprisingly in view of the sample preparation technique, these particles appear to be lying flat on the substrate with the Zr-Fe interface approximately perpendicular to the electron beam. If it is assumed that the Zr and Fe represent the cladding and immediately adjacent crud (as opposed to unrelated particles that became juxtaposed during sample preparation), the data indicate that hematite is the dominant iron oxide near the outer surface of the cladding, although the data in Figures 19a and b suggest the possible presence of one or more spinel minerals in addition to the hematite.

The hematite in Samples 21 and 22 occurs in a wide variety of crystal sizes and shapes, ranging from relatively large euhedral crystals such as those in Figures 4, 20, 27 to lath-shaped crystals such as those in Figure 17. Numerous methods for synthesizing essentially pure hematite in the laboratory are

known[5,6] and produce variations in crystal sizes and shapes comparable to those observed in these samples.

The SEM and TEM data suggest that Sample 11 contains two distinct kinds of clay (one with an Al:Si ratio slightly greater than 1:2 and one with a ratio of 1:1). Neither material seems likely to be part of the crud; however, Figures 10 and 14 suggest that it was collected as part of the sample rather than being introduced as a contaminant later. These materials may have been present in the pool, and been transported into the filter by the vacuum used to collect the samples. High-sodium and chloride-bearing phases are also unlikely in crud, and are probably contaminants. The origin of the corundum in Sample 21 (Cycle 16) is unknown, unless it represents fragments of the “stone” knife used to scrape the fuel pins during sample collection.

5. REFERENCES

1. Janney, D.E. and Porter, D.L., "Characterization of Phases in "Crud" from Boiling Water Reactors by Transmission Electron Microscopy," Manuscript submitted to Journal of *Nuclear Materials, 9 July 2006*.

2. Goldstein, J.I., Williams, D.B., and Cliff, G., 1986, "Quantitative X-ray Analysis," *Principles of Analytical Electron Microscopy*, D.C. Joy, A.D. Romig, Jr., and J.I Goldstein, eds, pp. 155-217, New York: Plenum.

3. Peacor, D.R., 1992, "Analytical Electron Microscopy: X-ray Analysis," *In Minerals and Reactions at the Atomic Scale: Transmission Electron Microscopy*, P.R. Buseck, ed. *Reviews in Mineralogy*, Vol. 27, pp. 113-140, Washington, D.C.: Mineralogical Society of America.

4. Kortright, J.B. and Thompson, A.C., 2001, "X-ray Properties of the Elements," *In X-ray Data Booklet, Center for X-Ray Optics and Advanced Light Source*, pp. 1-8 to 1-27, Lawrence Berkeley National Laboratory publication LBNL/Pub-490 Rev. 2.

5. Schwertmann, U. and Cornell, R.M., 2000, *Iron Oxides in the Laboratory*, ed. 2, Weinheim, Germany: Wiley-VCH.

6. Cornell, R.M. and Schwertmann, U., 2003, *The Iron Oxides: Structure, Properties, Reactions, Occurrences, and Uses*, ed. 2, Weinheim, Germany: Wiley-VCH.

Appendix A

Optical Images, Cycle 16

Appendix A

Optical Images, Cycle 16

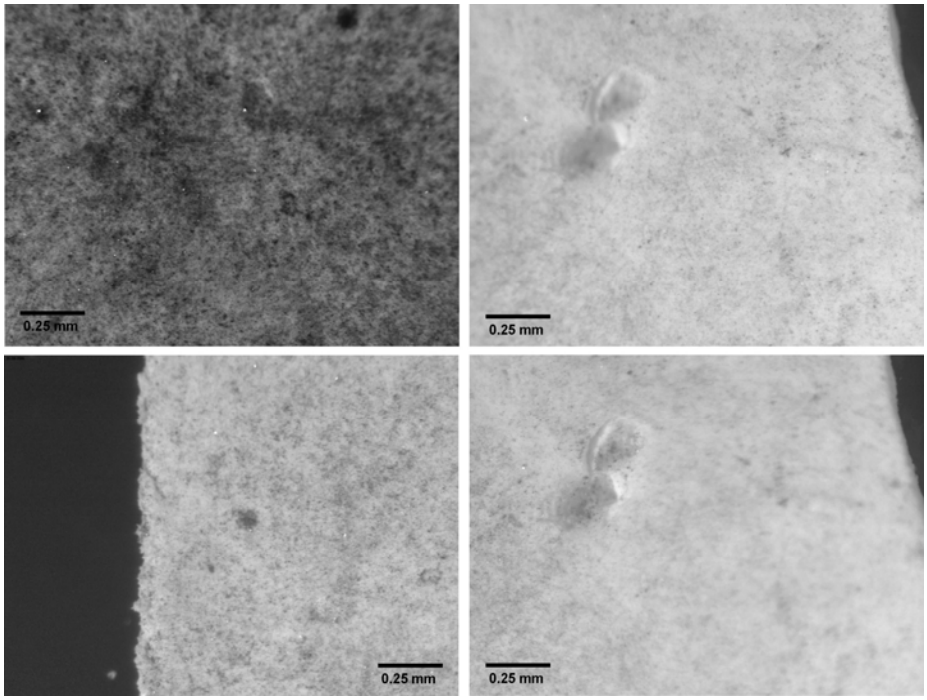

Figure A1. Optical images, Sample 21.

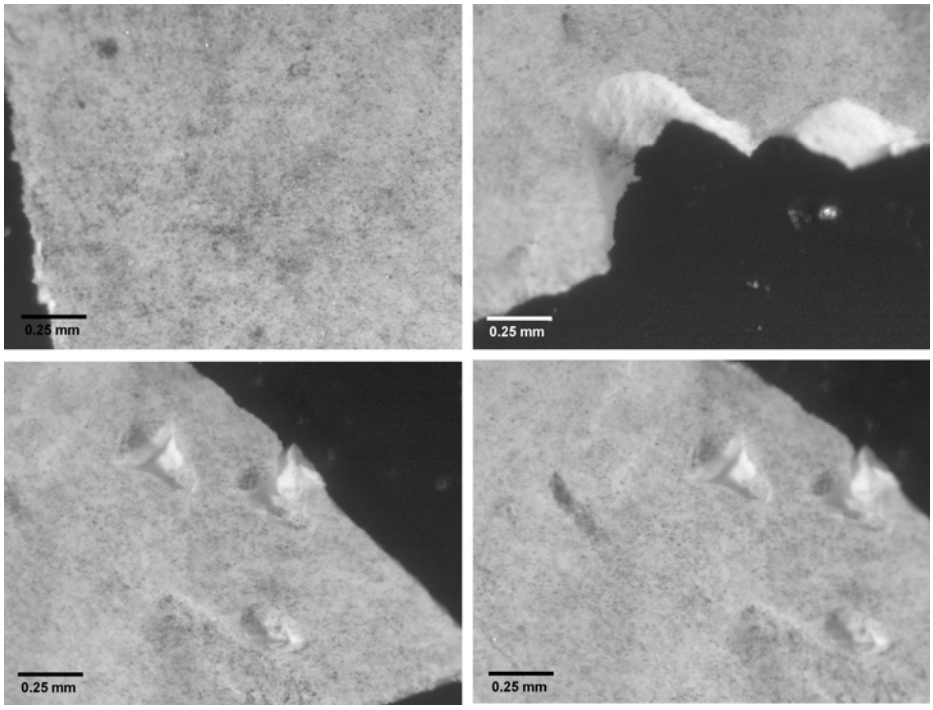

Figure A2. Optical images, Sample 21 (continued).

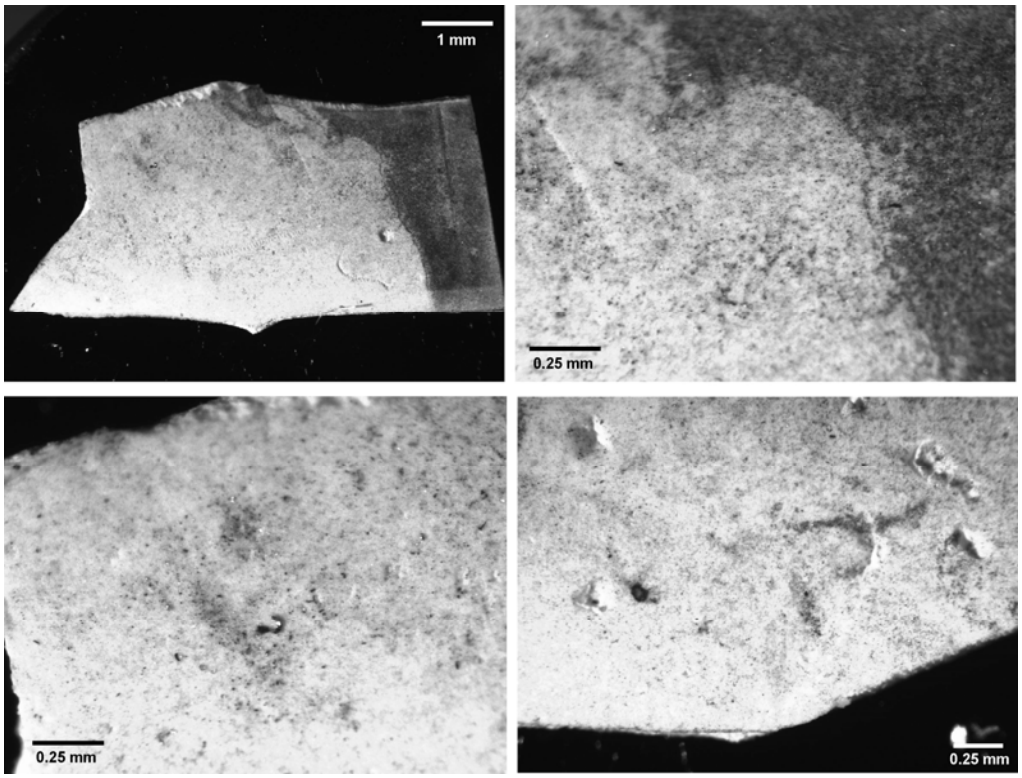

Figure A3. Optical images, Sample 22.

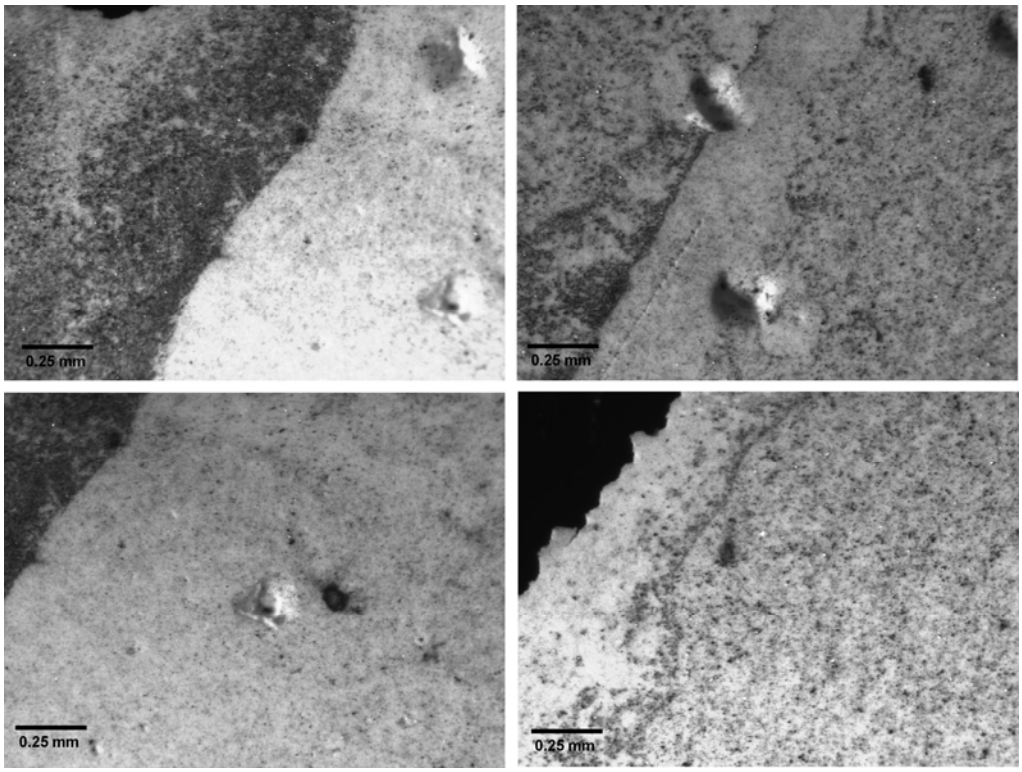

Figure A4. Optical images, Sample 22 (continued).

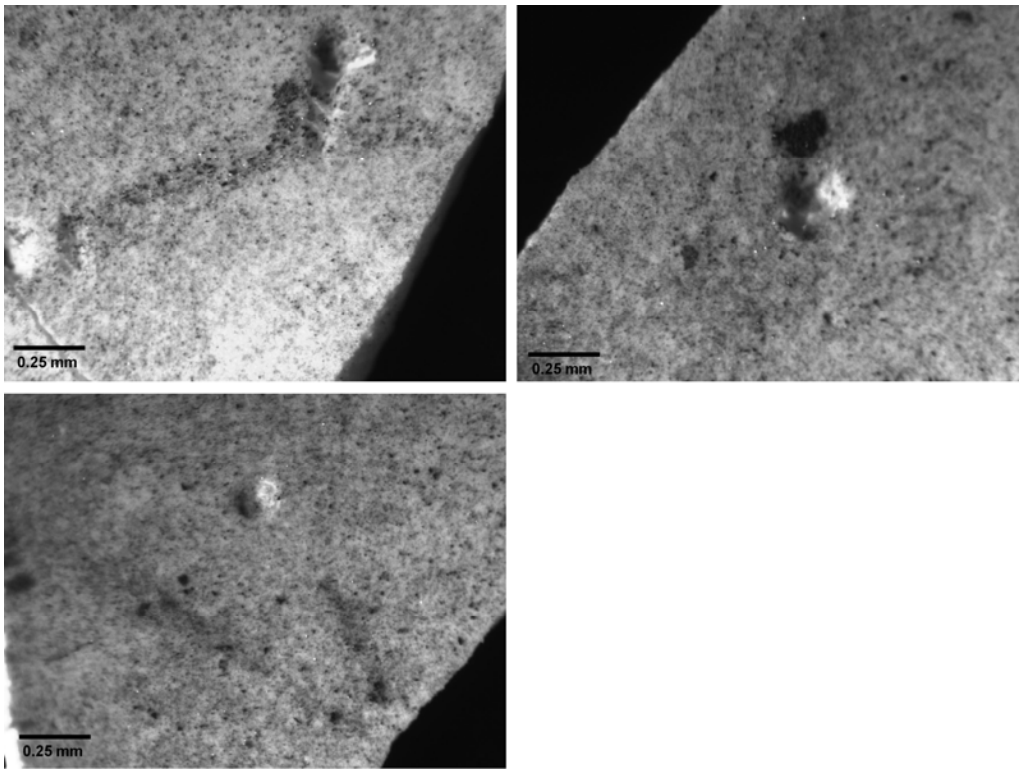

Figure A5. Optical images, Sample 22 (continued).

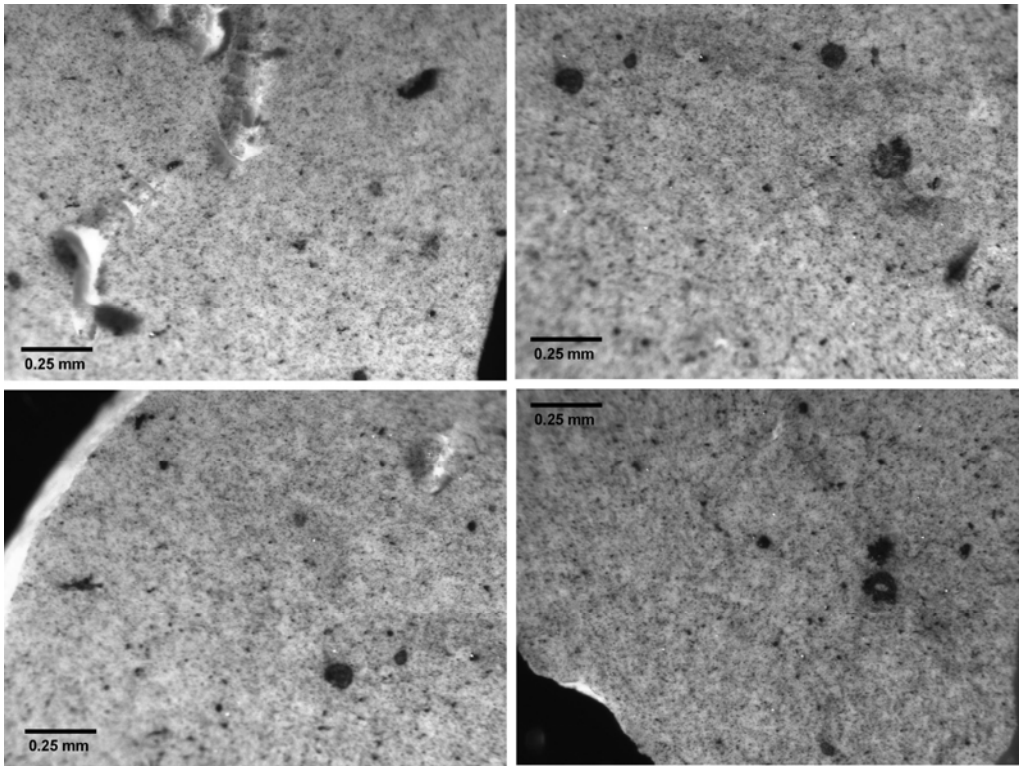

Figure A6. Optical images, Sample 25.

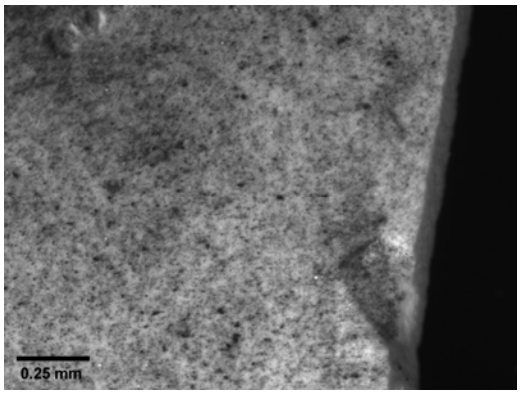

Figure A7. Optical images, Sample 25 (continued).

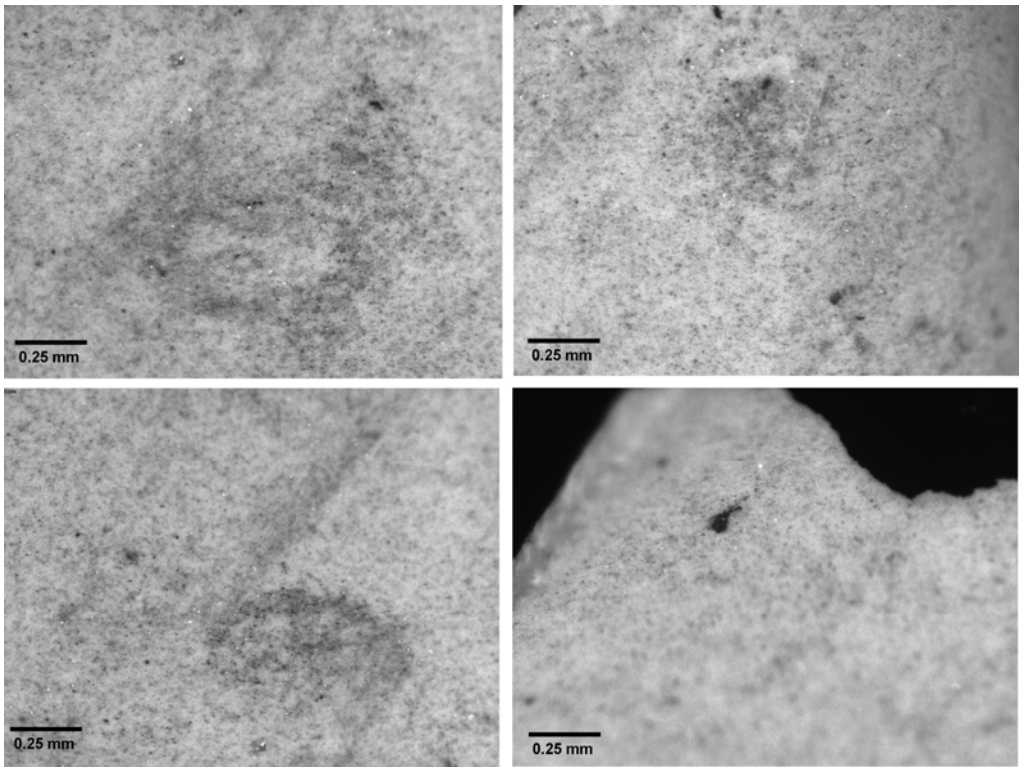

Figure A8. Optical images, Sample 28.

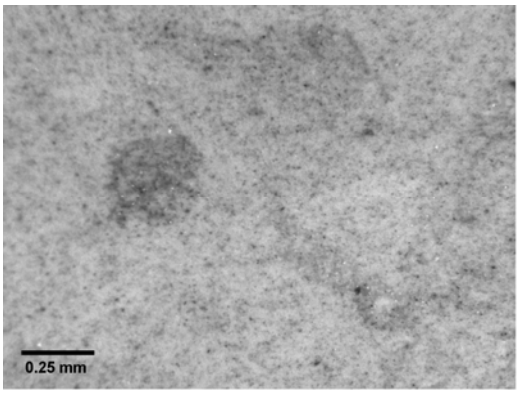

Figure A9. Optical images, Sample 28 (continued).

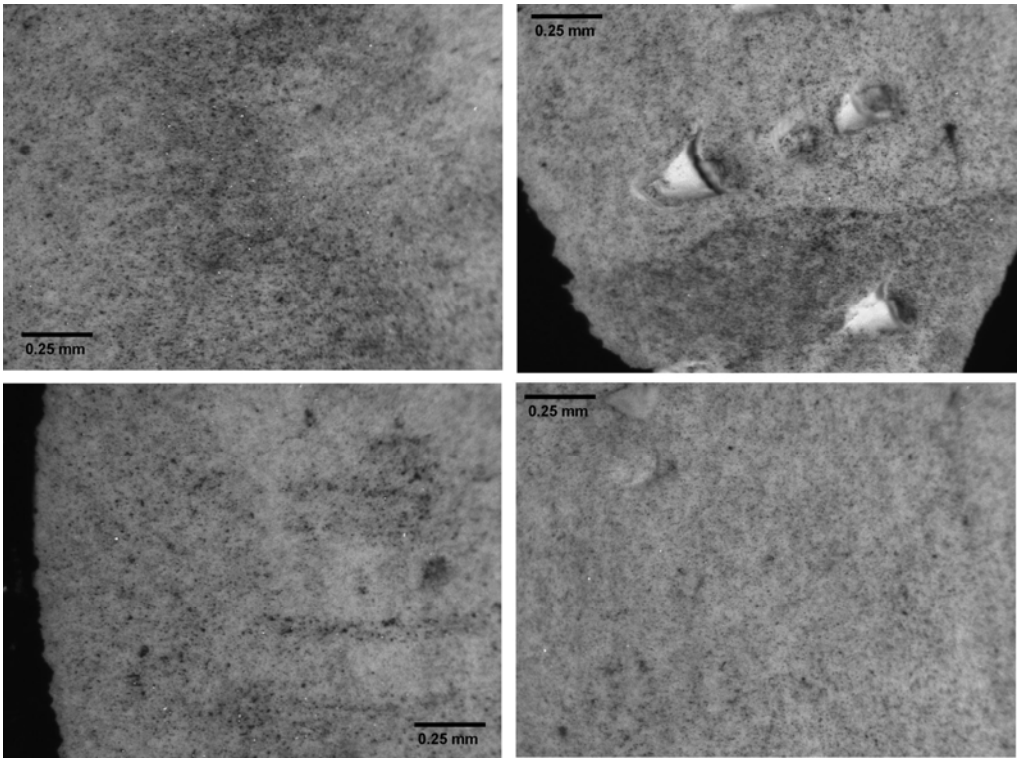

Figure A10. Optical images, Sample 29.

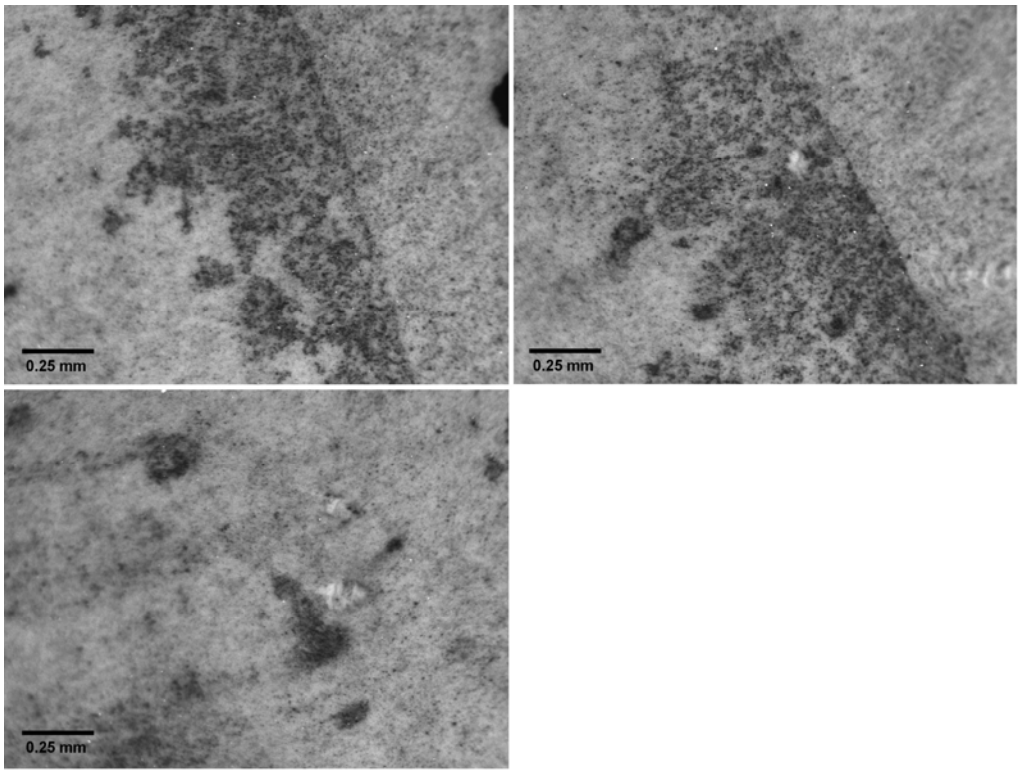

Figure A11. Optical images, Sample 29 (continued).

Appendix B

Weight percentages from SEM-EDX Spectra, Cycle 16 (Sample 21)

Appendix B

Weight percentages from SEM-EDX Spectra, Cycle 16 (Sample 21)

Table B-1. Weight percentages from SEM-EDX Spectra, Cycle 16 (Sample 21) (Normalized to 100%).

	Spectrum											
X-ray	29	30	31	32	33	34	35	36	37	38	39	40
Al K		100.0	0.3	0.8	100.0	1.6	100.0	1.8	10.4	1.3	100.0	8.3
Si K						0.9		0.2	1.2			2.6
Fe K						94.2						55.3
Ni K												2.7
Zr L	100.0		99.7	99.2		3.3		98.0	88.4	98.7		31.1

Appendix C

Weight percentages from TEM-EDX Spectra, Cycle 16 (Sample 21)

Appendix C

Weight percentages from TEM-EDX Spectra, Cycle 16 (Sample 21)

Table C-1. Weight percentages from TEM-EDX Spectra, Cycle 16 (Sample 21) (Normalized to 100%).

X-ray	Spectrum 2	Spectrum 3	Spectrum 4	Spectrum 5	Spectrum 6	Spectrum 7	Spectrum 8	Spectrum 9
Na K		4.9	2.9	7.6	1.7	5.7	42.9	5.1
Al K	18.1	22.9	1.3	2.8	0.5	2.5	1.5	81.3
Si K	75.5	59.5	2.7	11.8	1.9	8.3	29.9	3.4
Cl K							18.8	0.8
K K								
Ca K	6.5	10.9	0.9	2.7			4.5	
Fe K			7.2	10.9	5.2	13.7		2.3
Co K			2.0					
Ni K			0.7					
Cu K			0.5					
Zn K			0.4					
Sr K		1.7		0.7		0.5	2.4	0.3
Zr L			81.5	63.6	90.7	69.3		6.9
Ba L								

X-ray	Spectrum 34	Spectrum 35	Spectrum 36	Spectrum 37	Spectrum 38	Spectrum 39	Spectrum 40	Spectrum 41
Na K					6.4	8.5	4.9	4.6
Al K			94.8	96.3	3.0	2.2	3.0	3.8
Si K		0.7	2.5	1.6	3.7	17.2		12.5
Cl K					1.2	4.0	1.3	2.1
K K					0.5	1.5	0.4	
Ca K					1.3	3.2	2.5	2.8
Fe K	8.5	97.9	1.0	1.1	56.1	63.0	73.6	73.7
Co K			1.1	1.0				
Ni K		0.6			2.3			
Cu K	1.2	0.3			2.2		2.6	
Zn K					1.4			
Sr K					0.5	0.4	1.2	0.5
Zr L	90.2	0.6	0.7		17.1		2.8	
Ba L					4.3		7.7	

Appendix D

Analytical Lab results, Cycle 16

Appendix D

Analytical Lab results, Cycle 16

Tables D1 and D2 give composition and gamma-scan results for the Cycle 16 samples. Each sample was collected on a mixed cellulose ester filter. Although all of the filters were from the same lot number, and therefore, presumably had the same composition, no blank was available for analysis. Thus, all reported data include the filters used to collect the sample.

Table D1 gives quantities of K and Na measured by atomic absorption (AA) spectroscopy and concentrations of Al, Cr, Mn, Mo, Ni, Sr, Zn, and Zr measured by ion-coupled plasma mass spectroscopy (ICP-MS). Concentrations of Ca in each sample were below the detection limit for AA spectroscopy (~5 μg, but varying somewhat for different samples), and concentrations of U (all isotopes combined) were below the detection limit for ICP-MS (0.2 μg).

Table D1: Concentrations of analytes from Cycle 16 samples, μg. As specified in Table 1, samples in **bold** are pool samples not associated with specific rods or locations, samples in regular type are from Rod I9, and samples in *italics* are from Rod J6. Samples 4-9 were collected by brushing the fuel pins, while Samples 21-30 were collected by scraping.

	Element									
Sample	K	Na	Al	Cr	Mn	Mo	Ni	Sr	Zn	Zr
3	**568.4**	**102.5**		**8.96**	**1.16**		**15**	**0.64**	**39.1**	**113**
4	*545.8*	*80.8*		*53.6*	*26.2*	*0.782*	*105*	*0.17*	*71.1*	*89.7*
5	617.2	100.4		45.7	13.6	0.684	47.3	0.397		103
6	553.2	98.2		44.6	15.4	0.994	43.9	0.501		63.8
7	548	93.2		39	8.45		27.4	0.347		53.9
8	528.1	109		30.5	6.62		86.2	0.362		107
9	868.1	133.6		31.1	8.07		178	2.62	261	9.23
21	*608.5*	*112.9*		*45.3*	*22.7*	*1.64*	*62.1*	*0.435*	*54.6*	*3650*
22	655.3	155.7	206	49.7	19	1.69	52.2	0.547	50.4	3550
23	690.9	151.9		68.3	14.6	1.28	38.7	1.45	56.6	2760
24	*524.7*	*16.5*		*40.6*	*25.1*	*0.766*	*70.9*	*1.13*	*94.4*	*1540*
25	*586.1*	*2.4*		*71.9*	*29.2*	*3.76*	*428*	*0.507*	*89.9*	*2260*
26	535.6		1810	73.8	16	1.89	27.9	0.392	51.9	2340
27	569.1		320	67.6	23.8	2.66	59.9	1.13	79.5	4990
28	*540.9*	*34.1*	*630*	*55.1*	*10.5*		*12.3*	*1.02*		*75.6*
29	678.4			38.6	16.6	0.97			50.1	4250
30	*533.4*			*42.4*	*67.4*	*1.16*	*54.5*	*1.14*	*189*	*4180*
31	**508.6**			**10.9**	**1.64**			**0.369**		**382**

Table D2 gives activities of radioactive isotopes measured by gamma scans in August 2006. These activities differ from those at the time the crud formed because of ongoing radioactive decay processes.

As specified in Table 1, samples in bold are pool samples not associated with specific rods or locations, samples in regular type are from Rod I9, and samples in italics are from Rod J6. Samples 4-9 were collected by brushing the fuel pins, while Samples 21-30 were collected by scraping.

Table D2. Activities measured in August 2006 for Cycle 16 samples, μCi.

	Element			
Sample	Co-60	Mn-54	Zn-65	Sb-125
3	**0.259**			
4	*224*	*6.4*		
5	85	4.92		
6	51	3.39	1.15	
7	21.5	1.95		
8	11.5	0.63		
9	24.2	1.07		
21	*119*	*4.22*	*2.39*	
22	89	2.6		4.83
23	69	2.47	3.3	
24	*133*	*4.17*		
25	*139*	*4.42*	*2.44*	
26	66	2.27		
27	109	2.83		
28	*80*	*2.5*		
29	62	1.47	1.91	
30	*400*	*6.7*		
31	**7.8**	**0.318**		

Appendix E

Optical Images, Cycle 17

Appendix E

Optical Images, Cycle 17

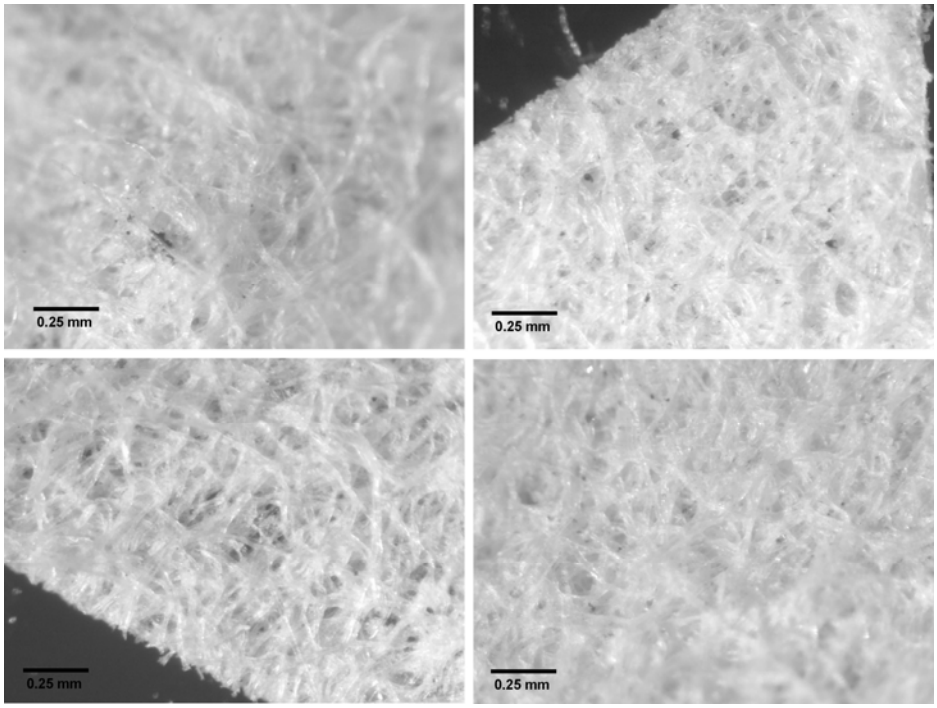

Figure E1. Optical images, Sample 11.

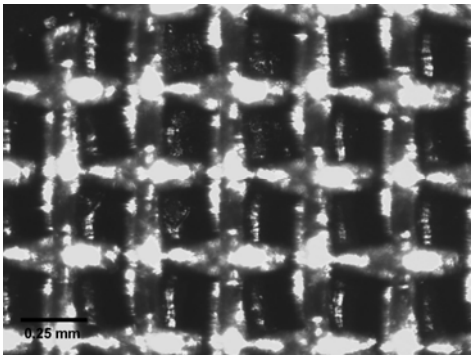

Figure E2. Optical image, Sample 12.

Appendix F

Weight Percentages from SEM-EDX Spectra, Cycle 17 (Sample 11)

Appendix F

Weight Percentages from SEM-EDX Spectra, Cycle 17 (Sample 11)

Table F-1. Weight Percentages from SEM-EDX Spectra, Cycle 17 (Sample 11) (Normalized to 100%).

X-ray	Spectrum 1	Spectrum 2	Spectrum 3	Spectrum 4	Spectrum 5
Al K		36.1			1.1
Si K		63.9			
Cr K					
Mn K					
Fe K	100.0		2.4	20.7	15.0
Ni K					
Zn K				2.2	
Zr L			91.7	77.1	83.9
Sn L			5.9		
Sb L					
Pb M					

X-ray	Spectrum 6	Spectrum 7	Spectrum 9	Spectrum 10
Al K				
Si K			4.2	1.1
Cr K				
Mn K				
Fe K	81.9	100.0		
Ni K	18.1			
Zn K				
Zr L				
Sn L				
Sb L			20.1	
Pb M			75.7	98.9

Table F-1. (continued).

X-ray	Spectrum 11	Spectrum 12	Spectrum 13	Spectrum 14
Al K			37.6	35.5
Si K	1.3	4.47	62.4	64.5
Cr K				
Mn K				
Fe K				
Ni K				
Zn K				
Zr L				
Sn L	10.1			
Sb L	22.2			
Pb M	76.4	95.4		

X-ray	Spectrum 16	Spectrum 17	Spectrum 18	Spectrum 19	Spectrum 20
Al K					
Si K					
Cr K					2.4
Mn K					2.1
Fe K	7.0	4.1	12.3	78.3	50.1
Ni K					16.3
Zn K					16.3
Zr L	93.0	95.9	87.7	21.7	12.8
Sn L					
Sb L					
Pb M					

Table F-1. (continued).

X-ray	Spectrum 21	Spectrum 22	Spectrum 23	Spectrum 24
Al K				
Si K				
Cr K				
Mn K				
Fe K	78.7	91.6	63.6	18.7
Ni K	7.1	3.6	11.2	
Zn K	10.2		14.8	
Zr L	4.0	4.8	10.4	81.3
Sn L				
Sb L				
Pb M				

X-ray	Spectrum 25	Spectrum 26	Spectrum 27	Spectrum 28
Al K				
Si K				
Cr K				
Mn K				
Fe K	100.0	9.5	71.8	8.8
Ni K			12.5	
Zn K			15.7	
Zr L		90.5		91.2
Sn L				
Sb L				
Pb M				

Appendix G

Weight Percentages from TEM-EDX Spectra, Cycle 17 (Sample 11)

Appendix G

Weight Percentages from TEM-EDX Spectra, Cycle 17 (Sample 11)

Table G-1. Weight Percentages from TEM-EDX Spectra, Cycle 17 (Sample 11) (Normalized to 100%)

X-ray	Spectrum 1	Spectrum 2	Spectrum 3	Spectrum 4	Spectrum 5
Na K		17.5	9.6		
Al K					
Si K	9.2	2.9	8.8	0.8	
Cl K					
K K					
Ca K	16.8	1.4	8.1	0.5	
Mn K				0.9	5.8
Fe K	73.7	78.1	73.6	89.2	37.4
Co K					
Ni K				2.5	9.8
Cu K				0.8	2.6
Zn K				3.3	14.2
Zr L	0.3	0.2		1.9	30.1
Pb L					

X-ray	Spectrum 6	Spectrum 7	Spectrum 8	Spectrum 9	Spectrum 10
Na K			29.0	9.3	5.5
Al K					
Si K		1.4		2.6	1.5
Cl K				1.4	
K K				1.8	
Ca K			14.3	3.3	
Mn K		8.9			
Fe K	5.3	49.7	40.1	29.6	20.2
Co K					
Ni K		11.9			5.5
Cu K	0.9	5.8		0.8	
Zn K		14.5	6.1	1.3	4.9
Zr L	93.9	7.9	10.7	50.0	62.4
Pb L					

Table G-1. (continued).

X-ray	Spectrum 11	Spectrum 12	Spectrum 13	Spectrum 14	Spectrum 15
Na K			18.4	1.5	
Al K					
Si K			2.9	1.4	
Cl K			4.0		
K K			1.7	0.2	
Ca K			5.6	0.2	
Ti K					
Cr K					
Mn K		0.8	0.4		
Fe K	17.7	95.0	55.0	9.8	
Co K					
Ni K	0.5	0.5	0.1		
Cu K	2.1				
Zn K	5.6		3.7	1.0	
Zr L	74.1	3.7	5.2	86.0	
Pb L			3.1		100.0

X-ray	Spectrum 16	Spectrum 17	Spectrum 18	Spectrum 19	Spectrum 20
Na K					
Al K					
Si K					
Cl K					
K K					
Ca K					
Ti K					
Cr K					
Mn K					
Fe K				100.0	9.4
Co K					
Ni K					0.2
Cu K					0.5
Zn K					
Zr L		100.0	100.0		89.9
Pb L	100.0				

Table G-1. (continued).

X-ray	Spectrum 21	Spectrum 22	Spectrum 23	Spectrum 24	Spectrum 25
Na K					13.3
Al K					25.0
Si K	1.7				2.5
Cl K	1.9				
K K	1.0				
Ca K	3.6	11.2			
Ti K					
Cr K					12.9
Mn K					
Fe K	83.3	88.9	100.0	100.0	
Co K					
Ni K					2.4
Cu K	1.6				0.8
Zn K	5.5				43.2
Zr L					
Pb L	1.3				

X-ray	Spectrum 26	Spectrum 27	Spectrum 28	Spectrum 29	Spectrum 30
Na K	9.4		6.4	10.0	12.8
Al K	11.5	5.3	8.3	11.2	27.4
Si K	6.4	5.4	2.2	6.5	7.7
Cl K					
K K					
Ca K		1.0	0.3		
Ti K					
Cr K	31.6	0.8	3.1	30.9	7.8
Mn K					
Fe K					
Co K					
Ni K	1.8	0.4	1.2	2.1	3.0
Cu K	0.8	1.2	1.1	1.0	1.3
Zn K	38.5	9.0	14.8	38.3	40.0
Zr L		77.0	62.7		
Pb L					

Table G-1. (continued).

X-ray	Spectrum 31	Spectrum 32	Spectrum 33	Spectrum 34	Spectrum 35
Na K		2.5	6.0	4.8	2.6
Al K	4.4				45.3
Si K	1.9	1.8	2.3	2.7	47.6
Cl K					1.1
K K					0.6
Ca K					0.4
Ti K					0.5
Cr K	16.5				
Mn K					
Fe K	50.5	91.8	84.8	86.6	1.8
Co K					
Ni K	21.8				
Cu K	4.8				
Zn K		4.0	6.9	5.9	
Zr L					
Pb L					

X-ray	Spectrum 36	Spectrum 37	Spectrum 38	Spectrum 39	Spectrum 40
Na K	0.8			30.2	1.2
Al K			0.8	3.5	
Si K	0.8	1.9		42.3	0.8
Cl K				15.2	
K K				2.8	
Ca K				5.9	
Ti K					
Cr K					0.7
Mn K		2.7			0.3
Fe K	98.3	63.4	99.2		94.2
Co K					2.2
Ni K		6.6			0.5
Cu K		6.2			0.2
Zn K		19.3			
Zr L					
Pb L					

Appendix H

Analytical Lab Results, Cycle 17

Appendix H

Analytical Lab Results, Cycle 17

Tables H1 and H2 give compositions and gamma scan results for the Cycle 17 samples. Concentrations of analytes measured from a blank filter paper comparable to that used to collect Samples 10 and 11 are also shown. Quantities of K in Table H1 were measured by AA spectroscopy, and the remaining elements in these tables were measured by ICP-MS. Concentrations of Ca and Na in all samples and the blank filter paper were below the detection limits for AA spectroscopy (~5 and 22 mg, respectively, but varying somewhat for different samples), and concentrations of U (all isotopes combined) were below the detection limit for ICP-MS (0.2 μg).

Table H2 gives activities of radioactive isotopes measured by gamma scans in August 2006. These activities differ from those at the time the crud formed because of ongoing radioactive decay processes.

Table H1. Concentrations of analytes from Cycle 17 samples collected on paper filters and blank filter, μg.

Sample	K	Cr	Mn	Mo	Ni	Sr	Zn	Zr
10	439	3.38	2.43			0.386	36.7	148
11	479.8	7.08	5.9			0.274		197
Blank	572	5.45	4.42		37.6	0.642	66.6	
12	524.5	3360	1100	300	13000	0.184		74.7

Table H2. Activities measured in August 2006 for Cycle 17 samples, μCi.

Sample	Co-60	Mn-54	Zn-65
10	19.2	5.2	2.29
11	23.2	4.85	3.21
12	4.99		